

Tracking Position and Orientation through Millimeter Wave Lens MIMO in 5G Systems

Arash Shahmansoori, Bernard Uguen, *Member, IEEE*, Giuseppe Destino, *Member, IEEE*,
Gonzalo Seco-Granados, *Senior Member, IEEE*, and Henk Wymeersch, *Member, IEEE*

Abstract

Millimeter wave signals and large antenna arrays are considered enabling technologies for future 5G networks. Despite their benefits for achieving high data rate communications, their potential advantages for tracking of the location of the user terminals are largely undiscovered. In this paper, we propose a novel support detection-based channel training method for frequency selective millimeter-wave (mm-wave) multiple-input-multiple-output system with lens antenna arrays. We show that accurate position and orientation estimation and tracking is possible using signals from a single transmitter with lens antenna arrays. Particularly, the beamspace channel estimation is formulated as two sparse signal recovery problems in the downlink and uplink for the estimation of angle-of-arrival, angle-of-departure, and time-of-arrival. The proposed method offers a higher sparse detection probability compared to the compressed sensing based solutions. Finally, a joint heuristic beamformer design and user position and orientation tracking approach are proposed based on initial estimation of channel parameters obtained in the training phase.

Index Terms

Arash Shahmansoori and Bernard Uguen are with the Institute of Electronics and Telecommunications of Rennes, Université de Rennes 1, 35042 Rennes, France, emails: arash.mansoori65@gmail.com and Bernard.Uguen@univ-rennes1.fr. Gonzalo Seco-Granados is with the Department of Telecommunications and Systems Engineering, Universitat Autònoma de Barcelona, 08193 Barcelona, Spain, email: gonzalo.seco@uab.cat. Henk Wymeersch is with the Department of Electrical Engineering, Chalmers University of Technology, 412 96 Gothenburg, Sweden, email: henkw@chalmers.se. Giuseppe Destino is with the center for wireless communications, University of Oulu, 90014 Oulu, Finland, and visiting research fellow at King's College London, email: giuseppe.destino@oulu.fi. This work was financially supported by M5HESTIA (mmW Multi-user Massive MIMO Hybrid Equipments for Sounding, Transmissions and HW ImplementAtion) project, the EU-H2020 project HIGHTS (High Precision Positioning for Cooperative ITS Applications) under grant nr. MG-3.5a-2014-636537, the VINNOVA COPPLAR project, funded under Strategic Vehicle Research and Innovation grant nr. 2015-04849, FALCON (Fundamental of simulataneous localization and communications) funded by the Academy of Finland, and R&D Projects of Spanish Ministry of Economy and Competitiveness TEC2017-89925-R. (Corresponding author: Arash Shahmansoori.)

5G networks, mm-wave, lens arrays, support detection-based channel training, position and orientation tracking, heuristic beamformer design.

I. INTRODUCTION

Mm-wave and massive multiple-input-multiple-output (MIMO) will likely be adopted technologies in fifth generation (5G) communication networks, thanks to a number of favorable properties. Particularly, due to exploiting the carrier frequencies beyond 30 GHz and large available bandwidth, mm-wave can provide high data rate. This can be obtained through dense spatial multiplexing with large antennas. [1], [2]. Despite the aforementioned properties that are desirable for 5G services, there are a number of challenges regarding mm-wave communications. One of the most important challenges is the severe path loss at high carrier frequencies. The loss in signal-to-noise ratio (SNR) is compensated through beamforming at the transmitter and/or receiver resulting in highly directional links [3]–[5]. The design of beamformers requires the knowledge of propagation channel, e.g., user position, scatterer locations, and so on. Since at mm-wave frequencies only the line-of-sight (LOS) and a few dominant multipath components contribute to the received signal power, the channel is sparse in the angular domain [6], [7]. In other words, diffuse scattering and multiple-bounce reflections are much weaker than LOS and single-bounce specular reflection [8]–[10]. Different methods for mm-wave channel estimation have been proposed by exploiting sparsity [11]–[19] and compressed sensing tools such as distributed compressed sensing-simultaneous orthogonal matching pursuit (DCS-SOMP) [20], compressive sampling matched pursuit (CoSOMP) [21], and group sparse compressed sensing (GCS) [22]. In [11], a method for channel parameter estimation is proposed based on the downlink compressive beacons. A compressed sensing (CS)-based method with redundant dictionary is proposed in [12]. A method based on hierarchical multi-resolution codebook design for the estimation of single-path and multi-path mm-wave channels is proposed in [13]. In [14], multiuser mm-wave MIMO channels with analog beamformers using a beam selection procedure is proposed. A CS-based method with reduced training overhead was considered in [15]. A robust algorithm with single feedback is used in [16]. A method based on CS tools with angular refinement is applied in [17], and continuous estimation of mm-wave channel parameters is proposed in [18]. In [19], CS tools are used for estimation of power-angle profiles of the mm-wave channels with overhead reduction compared to the codebook designs. In the aforementioned papers, a narrow-band mm-wave channel is considered. In this paper, we extend the results to the wideband mm-wave channel model, i.e., the delays of different paths are also estimated.

In mm-wave frequencies, and due to large number of antenna elements, equipping each antenna with a dedicated radio-frequency (RF)-chain is not cost-effective in terms of implementation and power consump-

tion. To reduce the number of RF-chains, there are two approaches. In the first approach, named as hybrid analog/digital processing, the digital precoding and combining is performed in the baseband followed by phase shifters in the RF band [23]. However, this approach may suffer from inefficiency of Power-Amplifier (PA) at high carrier frequency, non-linearity of PA, and heat dissipation and imbalances/non-ideality of the phase shifter responses. In the second approach, a low-cost implementation of mm-wave MIMO is achieved by using switching circuits together with lens antenna arrays [24]–[29]. To gain low-cost implementation with mm-wave lens MIMO, it is important to find efficient channel estimation methods. In mm-wave lens MIMO systems, the analog precoders are often in practice restricted to discrete Fourier transform (DFT) vectors [26]. Moreover, adopting traditional channel estimation techniques from hybrid analog/digital systems (e.g., the exhaustive and hierarchical search) for mm-wave lens MIMO systems does not lead to satisfying results. Different methods are proposed for mm-wave lens MIMO channel estimation in [28]–[30]. In [30], the sparsity mask detection (SMD) mm-wave lens MIMO channel estimation is proposed. In this approach, the beams with larger energy are detected with a beam training procedure between users and the base station (BS). Then, the dimension-reduced beamspace channel is estimated through least squares (LS) solutions. The computational complexity and pilot overhead in this method is reduced, however the number of required pilot symbols to scan all the beams is on the order of the number of antenna elements, e.g., 256 antennas. A similar approach based on energy based detection in uplink and downlink was used in [29]. In [28], the support detection (SD)-based estimation with reduced pilot symbols for narrowband mm-wave channel is proposed by exploiting the sparsity in the beamspace. The method performs better than the CS based approaches as it relies on the power detection. This results in better estimation capabilities at low SNR. However, the method is limited to the estimation of angle-of-arrival (AOA) and beamspace coefficients for the narrowband mm-wave lens MIMO channel.

The relative location of transmitter and receiver can be obtained using the estimated AOA/angle-of-departure (AOD) [31]. Moreover, the estimated user location provides necessary information for beamformer design. In other words, once the user location is estimated, the BS can steer the beam towards the user, either directly using the LOS path or through the first-order reflectors. This results in a synergy between localization and communication. The position and orientation estimation was previously explored in [32]–[34] and in [35]–[37] for mm-wave and massive MIMO systems, respectively. In [32], a beam switching approach was suggested for tracking of AOA. A link by link mm-wave AOA/AOD and channel gain tracking was proposed in [38], while a tracking solution for all the links was investigated in [39]. In [33], user localization was formulated as a hypothesis testing problem for a given spatial resolution. Meter-level positioning accuracy was obtained using the received signal strength levels in

[34]. To speed up initial access between nodes, a location-aided beamforming method was proposed in [40]. In the massive MIMO case, [35] considered the estimation of angles, a direct localization methods by jointly processing the observations at the distributed massive MIMO BSs was proposed in [41], while joint estimation of AOA/AOD and time-of-arrival (TOA) in the LOS with the impact of errors in delays and phase shifters was investigated in [36], sufficient conditions to obtain a non-singular Fisher information matrix (FIM) for delay, AOA/AOD and channel coefficients were derived in [42], and [43] proposed the corresponding estimators that approach position error bound (PEB) and rotation error bound (REB) for average to high SNR in the LOS, non-line-of-sight (NLOS), and obstructed-line-of-sight (OLOS) conditions. By linearizing the non-linear equations for time-difference-of-arrival (TDOA), AOA, and AOD, a hybrid localization approach was proposed in [44]. In [37], a Gaussian process regressor was applied to solve the positioning by operating on a vector of received signal strengths through fingerprinting. This approach does not harness the geometry of the environment, while it exploits the NLOS propagation. Complementarily to the use of mm-wave frequencies, approaches for localization using centimeter-wave (cm-wave) signals have been recently proposed as well. Joint TDOAs and AOAs using an extended Kalman filter (EKF) was proposed in [45], [46]. In this method, the mobile station (MS) has a single antenna and the BS employs an antenna array to provide sub-meter accuracy for moving devices. The main assumption is the LOS propagation thanks to high density of access nodes.

In this paper, we propose a position and orientation training method with one BS followed by the tracking phase. The method considers joint tracking of position and orientation together with beamformer design in the tracking phase initialized by the estimated values from the training phase. The main contributions of the paper are:

- A novel SD-based mm-wave channel estimation for frequency selective lens MIMO is proposed in the training phase. The main advantage of the proposed method over the traditional adopted CS-based (e.g., exhaustive and hierarchical search) mm-wave channel estimation approaches for lens MIMO is the increased detection probability of the sparse channel support, i.e., improved estimation accuracy. Moreover, the proposed method reduces the required time for training compared to the CS-based approaches.
- A position and orientation tracking method is proposed based on the EKF and the heuristic beamformer design in the tracking phase. The proposed method enables tracking of the position and rotation angle of the user with reduced number of required beams within the observation time.
- Joint heuristic beamformer and position and orientation training-tracking algorithm is proposed. From the simulation results, it is observed that the proposed algorithm provides comparable accuracies to

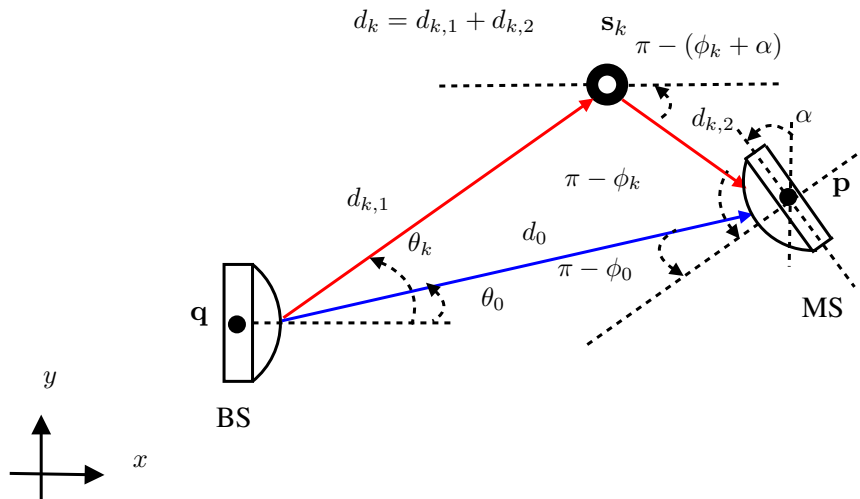


Fig. 1: Two dimensional illustration of the LOS (blue link) and NLOS (red link) based positioning problem. The BS location \mathbf{q} and BS orientation are known, but arbitrary. The unknown parameters include: the location of the MS \mathbf{p} , scatterer \mathbf{s}_k , rotation angle α , DL-AOAs $\{\phi_k\}$, UL-AOAs $\{\theta_k\}$, the channels between BS, MS, and scatterers, and the distance between the antenna centers.

the corresponding values of the PEB and REB even at low SNR.

II. SYSTEM MODEL

A MIMO system with a BS equipped with N_{BS} antennas and a MS equipped by N_{MS} antennas operating at a carrier frequency f_c (corresponding to wavelength λ_c) and bandwidth B has been considered. The BS and MS locations are denoted by $\mathbf{q} = [q_x, q_y]^T \in \mathbb{R}^2$ and $\mathbf{p} = [p_x, p_y]^T \in \mathbb{R}^2$. The rotation angle of the MS's antenna array is denoted by $\alpha \in [0, 2\pi)$. The location of the BS \mathbf{q} is assumed to be known, while \mathbf{p} and α are unknown and need to be estimated.

A. Transmitter Model

It is assumed that orthogonal frequency division multiplexing (OFDM) signals are used for transmission as in [47]. A BS with hybrid analog/digital precoder and lens array communicates with a single MS with lens array. The BS sequentially transmits G signals. The g -th transmission comprises M_{BS} simultaneously transmitted symbols $\mathbf{x}^{(g)}[n] = \frac{1}{\sqrt{M_{\text{BS}}}}[x_1[n], \dots, x_{M_{\text{BS}}}[n]]^T \in \mathbb{C}^{M_{\text{BS}}}$ for each subcarrier $n = 0, \dots, N-1$. The precoded symbols are transformed to the time-domain using N -point inverse fast Fourier transform (IFFT). A cyclic prefix (CP) of length $T_{\text{CP}} = DT_s$ is added before applying the RF precoding where D is the length of CP in symbols. The sampling period is defined as $T_s = 1/B$ and T_{CP} exceeds the

channel delay spread. The transmitted signal over subcarrier n at the g -th transmission can be expressed as $\mathbf{F}_{\text{RF,BS}}^{(g)} \mathbf{F}_{\text{BB,BS}}^{(g)} \mathbf{x}^{(g)}[n]$ where $\mathbf{F}_{\text{RF,BS}}^{(g)}$ is the analog precoder. The term $\mathbf{F}_{\text{BB,BS}}^{(g)}$ denotes the digital baseband precoder to compensate for imperfections of the desired beamformer design in the analog. The total power constraint $\|\mathbf{F}_{\text{RF,BS}}^{(g)} \mathbf{F}_{\text{BB,BS}}^{(g)}\|_{\text{F}} = 1$ is satisfied by the transmit beamformer.

B. Mm-Wave Lens MIMO Channel Model

Fig. 1 shows the position-related parameters of the channel including the location of the k -th scatterer \mathbf{s}_k , \mathbf{p} , and \mathbf{q} . Also, the corresponding channel parameters include ϕ_k , θ_k , and $d_k = c\tau_k$, denoting the AOA, AOD, and the path length (with TOA τ_k and the speed of light c) of the k -th path ($k = 0$ for the LOS path and $k > 0$ the NLOS paths). For the k -th NLOS path, we define $d_{k,1} = \|\mathbf{s}_k - \mathbf{q}\|_2$ and $d_{k,2} = \|\mathbf{p} - \mathbf{s}_k\|_2$. We consider a frequency-independent array response [7]. The channel is assumed to be constant during the transmission of G symbols in the downlink. Assuming $K + 1$ paths, the $N_{\text{MS}} \times N_{\text{BS}}$ mm-wave MIMO channel in the downlink is expressed as

$$\mathbf{H}_{\text{DL}}[n] = \mathbf{A}_{\text{MS}} \mathbf{\Gamma}[n] \mathbf{A}_{\text{BS}}^{\text{H}}, \quad (1)$$

where

$$\mathbf{A}_{\text{BS}} = [\mathbf{a}_{\text{BS}}(\theta_0), \dots, \mathbf{a}_{\text{BS}}(\theta_K)], \quad (2)$$

$$\mathbf{A}_{\text{MS}} = [\mathbf{a}_{\text{MS}}(\phi_0), \dots, \mathbf{a}_{\text{MS}}(\phi_K)], \quad (3)$$

$$\mathbf{\Gamma}[n] = \text{diag} \left\{ \gamma_n(\tilde{h}_0, \tau_0), \dots, \gamma_n(\tilde{h}_K, \tau_K) \right\}, \quad (4)$$

where $\gamma_n(\tilde{h}_k, \tau_k)$ is defined as $\gamma_n(\tilde{h}_k, \tau_k) = \tilde{h}_k e^{-j2\pi n \tau_k / (NT_s)}$ and $\tilde{h}_k = \sqrt{(N_{\text{BS}} N_{\text{MS}}) / \rho_k} h_k$ in which ρ_k denotes the path loss. The steering vector is defined as

$$\mathbf{a}_{\text{BS}}(\theta_k) = \frac{1}{\sqrt{N_{\text{BS}}}} [e^{-j \frac{N_{\text{BS}}-1}{2} \frac{2\pi}{\lambda_c} d \sin(\theta_k)}, \dots, e^{j \frac{N_{\text{BS}}-1}{2} \frac{2\pi}{\lambda_c} d \sin(\theta_k)}]^{\text{T}}. \quad (5)$$

The term $\mathbf{a}_{\text{MS}}(\phi_k)$ is defined similarly by replacing the subscript BS by MS, and θ_k by ϕ_k . The mm-wave lens MIMO channel model is obtained using DFT matrices \mathbf{U}_{BS} of size $N_{\text{BS}} \times N_{\text{BS}}$ and \mathbf{U}_{MS} of size $N_{\text{MS}} \times N_{\text{MS}}$ as¹ [28], [48]

$$\check{\mathbf{H}}_{\text{DL}}[n] = \mathbf{U}_{\text{MS}}^{\text{H}} \mathbf{H}_{\text{DL}}[n] \mathbf{U}_{\text{BS}} \quad (6)$$

$$= \sum_{k=0}^K \gamma_n(\tilde{h}_k, \tau_k) \mathbf{U}_{\text{MS}}^{\text{H}} \mathbf{a}_{\text{MS}}(\phi_k) \mathbf{a}_{\text{BS}}^{\text{H}}(\theta_k) \mathbf{U}_{\text{BS}}, \quad (7)$$

¹In principle, the electromagnetic lens can be approximately modeled with DFT matrices. An alternative approach is by integrating lens and antenna array as a single component [25].

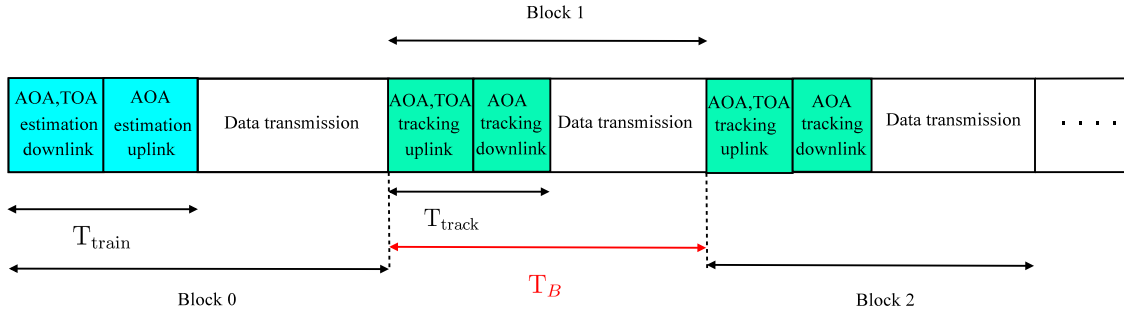


Fig. 2: The illustration of a training-tracking system with reduced training time and significant reduction of tracking time in the uplink and downlink.

where \mathbf{U}_{BS} contains N_{BS} orthogonal beams covering the entire angular domain as

$$\mathbf{U}_{\text{BS}} \triangleq [\mathbf{u}_{\text{BS}}(-(N_{\text{BS}} - 1)/2), \dots, \mathbf{u}_{\text{BS}}((N_{\text{BS}} - 1)/2)], \quad (8)$$

$$\mathbf{u}_{\text{BS}}(p) \triangleq \left[e^{-j2\pi \frac{N_{\text{BS}}-1}{2} \frac{p}{N_{\text{BS}}}}, \dots, e^{j2\pi \frac{N_{\text{BS}}-1}{2} \frac{p}{N_{\text{BS}}}} \right]^T, \quad (9)$$

and \mathbf{U}_{MS} is defined similarly by replacing the subscript BS with MS. It is readily verified that [7]

$$[\check{\mathbf{H}}[n]]_{\text{DL}, i, i'} = \sum_{k=0}^K \gamma_n(\tilde{h}_k, \tau_k) \chi_{\text{MS}}\left(\frac{d}{\lambda_c} \sin(\phi_k) - \frac{i}{N_{\text{MS}}}\right) \chi_{\text{BS}}\left(\frac{d}{\lambda_c} \sin(\theta_k) - \frac{i'}{N_{\text{BS}}}\right), \quad (10)$$

for $-(N_{\text{MS}} - 1)/2 \leq i \leq (N_{\text{MS}} - 1)/2$ and $-(N_{\text{BS}} - 1)/2 \leq i' \leq (N_{\text{BS}} - 1)/2$. We have introduced

$$\chi_{\text{BS}}(\phi) = \frac{\sin(\pi N_{\text{BS}} \phi)}{\sqrt{N_{\text{BS}}} \sin(\pi \phi)}, \quad (11)$$

$$\chi_{\text{MS}}(\phi) = \frac{\sin(\pi N_{\text{MS}} \phi)}{\sqrt{N_{\text{MS}}} \sin(\pi \phi)}. \quad (12)$$

Similarly, the uplink channel model in beamspace $\check{\mathbf{H}}_{\text{UL}}[n]$ is obtained by interchanging \mathbf{A}_{BS} and \mathbf{A}_{MS} in (1), and \mathbf{U}_{MS} and \mathbf{U}_{BS} in (6).

C. Received Signal in Beamspace

The downlink received signal is obtained as

$$\check{\mathbf{y}}^{\text{dl}, (g)}[n] = (\mathbf{F}_{\text{MS}}^{(g)})^H \check{\mathbf{H}}_{\text{DL}}[n] \mathbf{F}_{\text{BS}}^{(g)} \mathbf{x}^{(g)}[n] + \check{\mathbf{n}}_{\text{MS}}^{(g)}[n], \quad (13)$$

where $\check{\mathbf{H}}_{\text{DL}}[n]$ is the mm-wave lens MIMO channel in (6), $\mathbf{F}_{\text{MS}}^{(g)} = \mathbf{F}_{\text{RF}, \text{MS}}^{(g)} \mathbf{F}_{\text{BB}, \text{MS}}^{(g)}$ in which $\mathbf{F}_{\text{BB}, \text{MS}}^{(g)}$ and $\mathbf{F}_{\text{RF}, \text{MS}}^{(g)}$ are the digital baseband combiner and adaptive selecting network that is adaptively used as

an analog combiner during the channel estimation. The adaptive selecting network is implemented using 1-bit phase shifters² for choosing the antenna index of the lens array [28]. The noise vector is defined as

$$\check{\mathbf{n}}_{\text{MS}}^{(g)}[n] = (\mathbf{F}_{\text{MS}}^{(g)})^H \mathbf{U}_{\text{MS}}^H \mathbf{n}^{(g)}[n].$$

Finally, for G sequentially transmitted beams we obtain the downlink received signal

$$\check{\mathbf{y}}^{\text{dl}}[n] = \mathbf{\Omega}[n] \check{\mathbf{h}}[n] + \check{\mathbf{n}}_{\text{MS}}[n], \quad (14)$$

where

$$\mathbf{\Omega}[n] = \begin{bmatrix} \mathbf{\Omega}^{(1)}[n] \\ \vdots \\ \mathbf{\Omega}^{(G)}[n] \end{bmatrix}, \quad (15)$$

$$\mathbf{\Omega}^{(g)}[n] = (\mathbf{Z}_{\text{BS}}^{(g)}[n])^T \otimes (\mathbf{F}_{\text{MS}}^{(g)})^H, \quad (16)$$

$$\mathbf{Z}_{\text{BS}}^{(g)}[n] = \mathbf{F}_{\text{BS}}^{(g)} \mathbf{x}^{(g)}[n], \quad (17)$$

$$\check{\mathbf{h}}[n] = \text{vec}(\check{\mathbf{H}}_{\text{DL}}[n]). \quad (18)$$

Similarly, the uplink received signal is obtained by replacing the uplink channel model in the beamspace $\check{\mathbf{H}}_{\text{UL}}[n] = \mathbf{U}_{\text{BS}}^H \mathbf{H}_{\text{UL}}[n] \mathbf{U}_{\text{MS}}$ and interchanging $\mathbf{F}_{\text{BS}}^{(g)} = \mathbf{F}_{\text{RF,BS}}^{(g)} \mathbf{F}_{\text{BB,BS}}^{(g)}$ and $\mathbf{F}_{\text{MS}}^{(g)} = \mathbf{F}_{\text{RF,MS}}^{(g)} \mathbf{F}_{\text{BB,MS}}^{(g)}$ in (13). The terms $\mathbf{F}_{\text{BB,BS}}^{(g)}$ and $\mathbf{F}_{\text{RF,BS}}^{(g)}$ denote the digital baseband combiner and adaptive selecting network applied using 1-bit phase shifter in the BS, respectively. Consequently, the received signal for the sequential transmission of G signals in the uplink is obtained accordingly. Our goal is to provide a training-tracking system by uplink and downlink transmissions as shown in Fig. 2. In the training phase, i.e., Block 0, the main aim is to reduce the required time T_{train} for channel estimation. This leads to saving more symbols for data transmission and consequently increasing the data rate [49]. In the tracking phase, i.e., Block $m > 0$, instead of re-estimating the channel with the required time T_{train} , we propose an approach with significant reduction of training time, i.e. $T_{\text{track}} \ll T_{\text{train}}$. The duration of each block during the tracking phase is shown by³ T_B . Moreover, the localization information from the tracking phase helps the data transmission in a position-aided communication system.

²The adaptive selecting network can be applied for traditional beam selection in data transmission by turning off some phase shifters and setting the other phase shifters to zero to realize “unselect” and “select”, respectively. During beamspace channel estimation, it is adaptively used as an analog combiner to combine uplink or downlink signal.

³The value of T_B can be set to $T_B \approx d_0 / (v_{\text{max}} N_{\text{BS}})$ for the beamforming losses smaller than 3 dB at a given distance from the BS, d_0 , the maximum velocity v_{max} , and antenna element spacing $d = \lambda_c / 2$ for the worst case geometry [11]. Consequently, increasing v_{max} and N_{BS} leads to reducing T_B while increasing d_0 results increasing T_B .

III. CHANNEL ESTIMATION FOR LENS ANTENNA ARRAY

A novel extended SD-based method for frequency selective mm-wave MIMO channel is proposed for the estimation of channel parameters. In the training phase, it is assumed that the number of RF-chains in the BS and the MS are set to one, i.e., $M_{BS} = M_{MS} = 1$. The proposed method estimates the beamspace coefficients, AOA, TOA, and the number of channel paths K in the downlink phase. In the uplink phase, the AOA is estimated by the transmission of beams in the direction of the estimated AOA obtained from the downlink. The method directly estimates the beamspace channel coefficients. The proposed method performs better than the conventional CS-based approaches from the literature in terms of detection probability of the support of the sparse channel coefficient.

A. Background on SD-Based Method

The SD-based channel estimation method is an approach for the estimation of the mm-wave channel for the limited transmit power, i.e., low SNR [28]. In principle, the SD-based channel estimation method is based on the following properties for the beamspace channel coefficients:

- 1) Beamspace channel coefficients for different paths are asymptotically orthogonal for sufficiently large number of antenna elements.
- 2) The ratio between the power of V strongest elements of beamspace channel coefficient for a given path and the total power can be lower bounded. Moreover, the $V - 1$ strongest elements are located uniformly around the strongest element of beamspace channel coefficient.

Using the above properties, one can separately estimate the beamspace coefficients for different paths by starting from the strongest path and $V - 1$ strongest elements of beamspace channel coefficient, removing their effects and repeating the process until all the $\hat{K} + 1$ paths are estimated. Using the second property, it is possible to retain a few strongest elements of the beamspace channel coefficients for each path and set the rest of elements to zero without considerable power loss. Considering the second property, the support of the sparse channel coefficient is obtained with higher accuracy using the SD-based method compared to the traditional CS-based methods. This is due to the fact that in the CS-based methods only the position of strongest nonzero element of the sparse vector is obtained one by one for each path in an iterative way such that the magnitude and consequently the detection probability of strongest nonzero element for each path decreases [28].

B. Estimation of TOA/AOA and Beamspace Coefficients in the Downlink

To achieve desired recovery accuracy of the channel parameters for the training phase in the downlink, the adaptive selecting network in the MS, $\mathbf{F}_{RF,MS}^{(g)}$, is obtained using Bernoulli random matrix with

the elements randomly selected from $\{-1, +1\}$ with equal probability for each sequentially transmitted symbol, indexed by g . The baseband precoder $\mathbf{F}_{\text{BB,MS}}^{(g)}$ is populated with independent and identically distributed (i.i.d.) complex entries on the unit circle. This makes the mutual coherence between different columns of the sensing matrix as small as possible. The BS transmits equal power signal for all the elements of the lens antenna array. This is due to the fact that the AOD in the downlink is not estimated in this stage and the best AOD in the downlink to transmit highest signal power is not known a priori⁴. For equal power transmission in the BS without prior location information, one can use the RF-chain as a splitter⁵, i.e., $\mathbf{F}_{\text{RF,BS}}^{(g)} = \mathbf{1}_{N_{\text{BS}}}$, in the downlink. The received signal for the training phase in the downlink for the g -th sequentially transmitted symbol is simplified according to (13) as

$$\check{\mathbf{y}}^{\text{dl},(g)}[n] = x_{\text{BB,BS}}^{(g)}[n](\mathbf{F}_{\text{MS}}^{(g)})^{\text{H}}\check{\mathbf{h}}_{\text{MS}}[n] + \check{\mathbf{n}}_{\text{MS}}^{(g)}[n], \quad (19)$$

where⁶ $x_{\text{BB,BS}}^{(g)}[n] = F_{\text{BB,BS}}^{(g)}x^{(g)}[n]$ is the precoded signal for each subcarrier n and sequential index g . The term $\check{\mathbf{h}}_{\text{MS}}[n]$ is defined as

$$\check{\mathbf{h}}_{\text{MS}}[n] = \sqrt{N_{\text{BS}}} \sum_{k=0}^K \gamma_n(\check{h}_k, \tau_k) \boldsymbol{\chi}_{\text{MS},k}, \quad (20)$$

in which $\boldsymbol{\chi}_{\text{MS},k}$ is an $N_{\text{MS}} \times 1$ vector with the entries $\chi_{\text{MS}}\left(\frac{d}{\lambda_c} \sin(\phi_k) - \frac{i}{N_{\text{MS}}}\right)$ for $-(N_{\text{MS}} - 1)/2 \leq i \leq (N_{\text{MS}} - 1)/2$. In computing (19), we used the fact that

$$\boldsymbol{\chi}_{\text{BS},k}^{\text{T}} \mathbf{1}_{N_{\text{BS}}} = \sum_{i'=-\frac{N_{\text{BS}}-1}{2}}^{\frac{N_{\text{BS}}-1}{2}} \chi_{\text{BS}}\left(\frac{d}{\lambda_c} \sin(\theta_k) - \frac{i'}{N_{\text{BS}}}\right) \approx \sqrt{N_{\text{BS}}}, \quad \forall \theta_k \in [0, 2\pi) \quad (21)$$

where $\boldsymbol{\chi}_{\text{BS},k}$ is an $N_{\text{BS}} \times 1$ vector with the entries $\chi_{\text{BS}}\left(\frac{d}{\lambda_c} \sin(\theta_k) - \frac{i'}{N_{\text{BS}}}\right)$ for $-(N_{\text{BS}} - 1)/2 \leq i' \leq (N_{\text{BS}} - 1)/2$. Consequently, for G sequentially transmitted beams we obtain the $G \times 1$ received signal

$$\check{\mathbf{y}}^{\text{dl}}[n] = \boldsymbol{\Omega}_{\text{MS}}^{\text{H}}[n] \check{\mathbf{h}}_{\text{MS}}[n] + \check{\mathbf{n}}_{\text{MS}}[n], \quad (22)$$

where

$$\boldsymbol{\Omega}_{\text{MS}}[n] = \bar{\mathbf{F}}_{\text{MS}} \text{diag} \left\{ \left(x_{\text{BB,BS}}^{(1)}[n] \right)^*, \dots, \left(x_{\text{BB,BS}}^{(G)}[n] \right)^* \right\}, \quad (23)$$

where $\bar{\mathbf{F}}_{\text{MS}} = \left[\mathbf{F}_{\text{MS}}^{(1)}, \dots, \mathbf{F}_{\text{MS}}^{(G)} \right]$ denotes the $N_{\text{MS}} \times G$ sensing matrix with the i -th column vector $\mathbf{F}_{\text{MS}}^{(i)}$. Since there exist only a few non-zero elements in (20) for each path, $\check{\mathbf{h}}_{\text{MS}}[n]$ is a sparse vector. Consequently, the problem (22) can be considered as a sparse signal recovery with the sensing matrix

⁴This is equivalent to isotropical transmission [29].

⁵For the case of large number of antenna elements several splitters can be used for each subarray and the corresponding beams can be transmitted sequentially or simultaneously.

⁶Without loss of generality, one can choose $x_{\text{BB,BS}}^{(g)}[n] = 1$ for all g . This simplifies the sensing matrix in (23) as $\bar{\mathbf{F}}_{\text{MS}}$.

defined in (23). Moreover, since $\bar{\mathbf{F}}_{\text{MS}}$ is designed to exhibit low mutual coherence among its columns, by choosing random phase shifters for both RF and baseband parts, it is guaranteed that the complete information is available even for the values of G much less than N_{MS} . In particular to solve (22), the number of sequentially transmitted signals⁷ should satisfy $G \succeq (\hat{K} + 1) \log(N_{\text{MS}}/(\hat{K} + 1))$ [50].

The channel estimation in the downlink is explained in Algorithm 1. The received signal in the downlink $\check{\mathbf{y}}^{\text{dl}}[n]$ in (22), sensing matrix $\mathbf{\Omega}_{\text{MS}}[n]$ in (23), the required number of strongest elements V , and the threshold δ are the input parameters. The output parameters are the estimates of K , ϕ_k , and $\check{\mathbf{h}}_{\text{MS}}[n]$ for $n = 0, \dots, N-1$. First, the values of the residual vector $\mathbf{r}_t^{\text{dl}}[n]$ and beamspace channel coefficient $\check{\mathbf{h}}_{\text{MS},t}[n]$ are initialized as, $\mathbf{r}_{-1}^{\text{dl}}[n] = \mathbf{0}_{N_{\text{MS}}}$, $\mathbf{r}_0^{\text{dl}}[n] = \check{\mathbf{y}}^{\text{dl}}[n]$, and $\check{\mathbf{h}}_{\text{MS},t}[n] = \mathbf{0}_{N_{\text{MS}}}$, respectively. The corresponding index of the t -th AOA is estimated by finding the maximum value of the inner product of the m_{MS} -th row of sensing matrix $\mathbf{\Omega}_{\text{MS}}[n]$ defined as $\omega_{\text{MS},m_{\text{MS}}}$ and the residual vector $\mathbf{r}_t^{\text{dl}}[n]$ for $m_{\text{MS}} = 1, \dots, N_{\text{MS}}$ in (25). Consequently, the AOA is obtained based on (26). The support region for the corresponding index $\tilde{m}_{\text{MS},t}$ is computed based on SD-based approach for the even number of strongest elements⁸ V in (27) where the operation $\text{mod}_{N_{\text{MS}}} \{.\}$ ensures the support not to exceed N_{MS} . Next, the beamspace channel coefficient for the t -th path $\check{\mathbf{h}}_{\text{MS},t}[n]$ is computed based on the LS solution for (22) obtained as (28). Consequently, the residual vector $\mathbf{r}_{t-1}^{\text{dl}}[n]$ is updated by subtracting the effect of corresponding path from the previous residual vector $\mathbf{r}_t^{\text{dl}}[n]$ in (29) and the iteration index t is increased by 1. Finally, the aforementioned steps are repeated until the stopping criteria defined as $\sum_{n=0}^{N-1} \|\mathbf{r}_{t-1}^{\text{dl}}[n] - \mathbf{r}_t^{\text{dl}}[n]\|_2^2 > \delta$ is fulfilled for a given threshold δ . The threshold δ is obtained using constant false alarm rate (CFAR) test with a similar procedure as in [11]:

$$\delta = N_0 \gamma^{-1} \left(N, \Gamma(N) (1 - \mathbb{P}_{\text{fa}})^{1/N_{\text{MS}}} \right), \quad (24)$$

where $\gamma^{-1}(N, x)$ denotes the inverse of the incomplete gamma distribution, $\Gamma(N)$ is the gamma function, and \mathbb{P}_{fa} is the false alarm probability. Using the estimated values of the beamspace coefficients $\check{\mathbf{h}}_{\text{MS},t}[n]$ for $n = 0, \dots, N-1$, $\gamma_n(\tilde{h}_k, \tau_k)$ and consequently \tilde{h}_k and τ_k are estimated for each path $k = 0, \dots, \hat{K}$ based on a similar LS solution as in [43].

⁷For compactness, Hardy's notation is used [50].

⁸For the odd number of strongest elements V and the t -th path, the support would be $\text{supp}(\chi_{\text{MS},t}) = \text{mod}_{N_{\text{MS}}} \left\{ \tilde{m}_{\text{MS},t} - \frac{V-1}{2}, \dots, \tilde{m}_{\text{MS},t} + \frac{V-1}{2} \right\}$. In principle, the value of V is not known a priori and can be set to a fixed number for a given energy detection ratio.

Algorithm 1: Extended SD-Based Channel Estimation in the Downlink

Input : Received signals $\check{\mathbf{y}}^{\text{dl}}[n]$, sensing matrix $\mathbf{\Omega}_{\text{MS}}[n]$, required number of strongest elements V , and the threshold δ .

Output: estimates of K , ϕ_k , and $\hat{\mathbf{h}}_{\text{MS},k}[n]_{\text{supp}(\mathbf{x}_{\text{MS},k})}$ for $n = 0, \dots, N - 1$.

1 **Initialization:** For $n = 0, \dots, N - 1$ and $t = 0$, the residual vectors and beamspace coefficients are set to $\mathbf{r}_{-1}^{\text{dl}}[n] = \mathbf{0}_{N_{\text{MS}}}$, $\mathbf{r}_0^{\text{dl}}[n] = \check{\mathbf{y}}^{\text{dl}}[n]$, and $\hat{\mathbf{h}}_{\text{MS},0}[n] = \mathbf{0}_{N_{\text{MS}}}$;

2 **while** $\sum_{n=0}^{N-1} \|\mathbf{r}_{t-1}^{\text{dl}}[n] - \mathbf{r}_{t-2}^{\text{dl}}[n]\|_2^2 > \delta$ **do**

- Find AOA in the downlink

$$\tilde{m}_{\text{MS},t} = \underset{m_{\text{MS}}=1,\dots,N_{\text{MS}}}{\text{argmax}} \sum_{n=0}^{N-1} \frac{|\boldsymbol{\omega}_{\text{MS},m_{\text{MS}}}^{\text{H}}[n] \mathbf{r}_{t-1}^{\text{dl}}[n]|}{\|\mathbf{f}_{\text{MS},x,m_{\text{MS}}}[n]\|_2}, \quad (25)$$

$$\hat{\phi}_t = \arcsin((\lambda_c/d)(\tilde{m}_{\text{MS},t} - (N_{\text{MS}} - 1)/2 - 1)/N_{\text{MS}}). \quad (26)$$

- Compute the sparsity support with the even number of elements V as

$$\text{supp}(\mathbf{x}_{\text{MS},t}) = \text{mod}_{N_{\text{MS}}} \left\{ \tilde{m}_{\text{MS},t} - \frac{V}{2}, \dots, \tilde{m}_{\text{MS},t} + \frac{V-2}{2} \right\}. \quad (27)$$

- Compute $\hat{\mathbf{h}}_{\text{MS},t}[n]$ for $n = 0, \dots, N - 1$ as

$$\hat{\mathbf{h}}_{\text{MS},t}[n]_{\text{supp}(\mathbf{x}_{\text{MS},t})} = [\mathbf{\Omega}_{\text{MS}}]_{(:,\text{supp}(\mathbf{x}_{\text{MS},t}))}^{\dagger} [n] \mathbf{r}_{t-1}^{\text{dl}}[n]. \quad (28)$$

- Update the residual vector $\mathbf{r}_t^{\text{dl}}[n]$ for $n = 0, \dots, N - 1$ as

$$\mathbf{r}_t^{\text{dl}}[n] = \mathbf{r}_{t-1}^{\text{dl}}[n] - \mathbf{\Omega}_{\text{MS}}[n] \hat{\mathbf{h}}_{\text{MS},t}[n]_{\text{supp}(\mathbf{x}_{\text{MS},t})}. \quad (29)$$

- Set $t = t + 1$.

3 **end**

C. Estimation of AOA in the Uplink

In the uplink, the AOA is estimated⁹ by the sequential transmission with one RF-chain in the MS, i.e., $M_{\text{MS}} = 1$. In the uplink the BS has no knowledge of the AOA and applies the analog combiner $\mathbf{F}_{\text{RF,BS}}^{(g)}$ using the Bernoulli random matrix with the elements randomly selected from $\{-1, +1\}$ with equal probability. Similar to the downlink, $\mathbf{F}_{\text{BB,BS}}^{(g)}$ is set to i.i.d. complex entries populated on the unit circle. This makes the mutual coherence between different columns of the sensing matrix as small as possible

⁹To reduce the complexity, it is assumed that there is no clock bias in the BS or MS, consequently the TOA is only estimated in the downlink with no need for bias compensation using two-way TOA estimation protocols.

similar to the downlink. The received signal for the training phase in the uplink is simplified as

$$\check{\mathbf{y}}^{\text{ul}}[n] = \mathbf{\Omega}_{\text{BS}}^{\text{H}}[n]\check{\mathbf{h}}_{\text{BS}}[n] + \check{\mathbf{n}}_{\text{BS}}[n], \quad (30)$$

where

$$\mathbf{\Omega}_{\text{BS}}[n] = \bar{\mathbf{F}}_{\text{BS}} \text{diag} \left\{ \left(x_{\text{BB,MS}}^{(1)}[n] \right)^*, \dots, \left(x_{\text{BB,MS}}^{(G)}[n] \right)^* \right\}, \quad (31)$$

in which $\bar{\mathbf{F}}_{\text{BS}} = \left[\mathbf{F}_{\text{BS}}^{(1)}, \dots, \mathbf{F}_{\text{BS}}^{(G)} \right]$ denotes the $N_{\text{BS}} \times G$ sensing matrix with the i -th column vector $\mathbf{F}_{\text{BS}}^{(i)}$, and $x_{\text{BB,MS}}^{(g)}[n] = F_{\text{BB,MS}}^{(g)} x^{(g)}[n]$ is the precoded signal in the MS. The term $\check{\mathbf{h}}_{\text{BS}}[n]$ in (30) denotes

$$\check{\mathbf{h}}_{\text{BS}}[n] = \sqrt{N_{\text{MS}}} \sum_{k=0}^K \gamma_n(\tilde{h}_k, \tau_k) \mathbf{\chi}_{\text{BS},k}, \quad (32)$$

where we used a similar principle as in (21) using an all-one precoder in the MS. The problem (30) is considered as a sparse signal recovery with the sensing matrix defined in (31), since there exist only a few non-zero elements in (32) for each path. Using the received signal in the uplink $\check{\mathbf{y}}^{\text{ul}}[n]$ in (30), the AOAs in the uplink are estimated with the same principle as in Section III-B, for $\hat{K} + 1$ paths accounting for all subcarriers¹⁰. Moreover, the angular refinement can be achieved using a similar procedure as in [43]. Finally, the proposed method can be easily extended for the multiuser channel training by repeating the same procedures with randomly selected signals in the uplink and downlink for each user.

The complexity analysis of different steps of the training phase is proposed in the Appendix VIII.

D. Required Time for Training

The required time for channel training using the proposed method is significantly reduced compared to traditional methods. The traditional methods including exhaustive sequential transmission in N_{BS} directions and exhaustive sequential reception in N_{MS} directions, and hierarchical codebook designs with progressively broader beams with N_{RF} RF chains require the training times of $T_{\text{train}} = T_s N_{\text{BS}} N_{\text{MS}}$ and $T_{\text{train}} = T_s M_G (\hat{K} + 1)^2 \lceil \frac{M_G (\hat{K} + 1)}{N_{\text{RF}}} \rceil \log_{\frac{N_G}{M_G}}^{\frac{N_G}{\hat{K} + 1}}$ where N_G is the term denoting the grid resolution $2\pi/N_G$ and M_G denotes the number of precoders, respectively [13]. On the contrary, the proposed method requires the training time of GT_s in the downlink and GT_s in the uplink and the total training time of $T_{\text{train}} = 2GT_s$ where $G \succeq (\hat{K} + 1) \log(N_{\text{BS/MS}}/(\hat{K} + 1))$. Moreover, the detection probability of the support of the sparse channel coefficient (i.e., the estimation accuracy) of the proposed method is better than the corresponding adopted CS-based solutions for lens antenna arrays especially for low SNR as will be explained in the

¹⁰In principle, the angular sparsity pattern does not change for different subcarriers provided that the conditions in [7], [43] hold. Consequently, it is sufficient to consider a few subcarriers in the uplink in practice. Nevertheless, if this is not the case due to beam squint, the Algorithm 1 needs to be repeated for each subcarrier. A procedure for an antenna array at the BS and a single antenna at the MS considering the effect of beam squint was proposed in [51].

simulations. Following the above discussion, one can save several symbols from channel training for different purposes during the mm-wave channel coherence time¹¹, e.g., communication, localization, and so on. After changing channel parameters due to different reasons, e.g., user movement, the estimated values from the training phase are not valid anymore. In this case, instead of re-estimating channel parameters with small changes that is complex and costly, we propose a tracking phase in the next section.

IV. TRACKING OF CHANNEL PARAMETERS AND POSITION AND ORIENTATION

In this section we propose a tracking approach based on the EKF method for channel parameters and position and orientation based on the information provided by the LOS link¹². It is assumed that the BS does not move and tracks the location of the MS, and the MS tracks its rotation angle using the location information provided by the BS.

A. Measurement and State Equations

A continuous white noise acceleration (CWNA) model is employed for the state evolution for tracking AOA/AOD, and TOA [52]. The state vector for the LOS path can be written as¹³

$$\boldsymbol{\psi}_0^{[m]} = \left[(\boldsymbol{\eta}_0^{[m]})^T \quad (\dot{\boldsymbol{\eta}}_0^{[m]})^T \right]^T, \quad (33)$$

where $\boldsymbol{\eta}_0^{[m]} = [\tau_0^{[m]}, \theta_0^{[m]}, \phi_0^{[m]}]^T$ and $\dot{\boldsymbol{\eta}}_0^{[m]} = [\dot{\tau}_0^{[m]}, \dot{\theta}_0^{[m]}, \dot{\phi}_0^{[m]}]^T$. The terms $\theta_0^{[m]}$ and $\phi_0^{[m]}$ denote the AOD and AOA for the LOS path at the time instant m , respectively. Similarly, $\tau_0^{[m]}$ denotes the TOA for the LOS path. Finally, the parameters $\dot{\tau}_0^{[m]}$, $\dot{\theta}_0^{[m]}$, and $\dot{\phi}_0^{[m]}$ denote the rate-of-change of the TOA, AOD, and AOA for the block duration T_B , respectively. Assuming CWNA model, the state evolution model can be written as

$$\boldsymbol{\psi}_0^{[m]} = \boldsymbol{\Phi} \boldsymbol{\psi}_0^{[m-1]} + \mathbf{u}_0^{[m]}, \quad (34)$$

where $\mathbf{u}_0^{[m]}$ denotes the state noise with $\mathbb{E} \left[\mathbf{u}_0^{[m]} (\mathbf{u}_0^{[m]})^T \right] = \mathbf{Q}_0^{[m]}$. In general, the bi-azimuth generalized Von-Mises-Fisher (VMF) distribution for joint AOA/AOD or its approximation by a 2-D truncated

¹¹The time that mm-wave channel does not change (i.e., coherence time) is usually small due to large f_c . However, it includes several symbols thanks to the large bandwidth.

¹²In the tracking phase, one can use the estimated channel parameters from the NLOS links obtained from the training phase for location estimation of stationary first-order reflectors, i.e., mapping the environment [43].

¹³Note that for tracking user location and orientation channel coefficient \tilde{h}_0 acts as a nuisance parameter and can be omitted from the state vector to reduce the computational complexity. This is due to the fact that AOA/AOD and TOA obtained from the LOS are sufficient for position and orientation estimation. Equivalently, the state vector can be written for position and rotation angle and converted to the channel parameters after tracking.

Gaussian pdf for slightly distributed path components can be applied for directional data [53], [54]. In this case, we applied the approximation with a 2-D truncated Gaussian pdf with σ_{ϕ_0} , σ_{θ_0} , and $\rho_{\theta\phi,0}$ denoting the direction spreads of the AOA, AOD, and cross correlation for the LOS path, respectively. Moreover, the amount of noise would depend on T_B , the time between pilot transmissions. The state transition matrix $\Phi \in \mathbb{R}^{6 \times 6}$ is defined as

$$\Phi = \begin{bmatrix} \mathbf{I}_3 & T_B \mathbf{I}_3 \\ \mathbf{0}_3 & \mathbf{I}_3 \end{bmatrix}. \quad (35)$$

For $m = 1$, the entries of $\psi_0^{[m-1]}$ in (34) are initialized as: $\tau_0^{[0]} = \hat{\tau}_0$, $\phi_0^{[0]} = \hat{\phi}_0$, and $\theta_0^{[0]} = \hat{\theta}_0$ where $\hat{\tau}_0$, $\hat{\phi}_0$, and $\hat{\theta}_0$ are obtained from the training phase. The rate-of-change terms are initialized¹⁴ by two consecutive estimates of $\eta_0[m] = [\tau_0^{[m]}, \theta_0^{[m]}, \phi_0^{[m]}]^T$ as: $\dot{\tau}_0^{[1]} = (\tau_0^{[1]} - \tau_0^{[0]})/T_B$, $\dot{\theta}_0^{[1]} = (\theta_0^{[1]} - \theta_0^{[0]})/T_B$, and $\dot{\phi}_0^{[1]} = (\phi_0^{[1]} - \phi_0^{[0]})/T_B$. For tracking of the channel parameters, the EKF is applied with the state comprising the LOS delay, DL-AOA, UL-AOA, and their corresponding rates of changes, with the linear process model and nonlinear measurement equations in the downlink and the uplink. The measurement equation in the uplink¹⁵ is obtained for all the subcarriers (with the designed beamformers in the BS and the MS directed towards the LOS link as will be explained in the next section) as

$$\tilde{\mathbf{y}}_r^{\text{ul},[m]} = \vartheta_0^{\text{ul}}(\eta_0^{[m]}) + \sum_{l=1}^{\hat{K}} \vartheta_0^{\text{ul}}(\eta_l^{[m]}) + \tilde{\mathbf{n}}_{\text{BS}}^{[m]}. \quad (36)$$

In (36), the second term denotes the superposition of all the other NLOS paths acting as an added term to the measurement noise $\tilde{\mathbf{n}}_{\text{BS}}^{[m]} = \mathbf{F}_{\text{BS},0}^H \tilde{\mathbf{n}}^{[m]}$ where $\mathbf{F}_{\text{BS},0}$ is obtained based on the robust/heuristic design explained in the next section. The TOA-AOA are the parameters to be tracked for the block index m in the BS, and $\vartheta_0^{\text{ul}}(\eta_l^{[m]})$ denotes

$$\vartheta_0^{\text{ul}}(\eta_k^{[m]}) = \tilde{h}_k^{[m]} \left(\mathbf{X}_0^T (\mathbf{F}_{\text{MS},0}^{[m-1]})^T \chi_{\text{MS},k}^{[m]} \odot \mathbf{a}(\tau_k^{[m]}) \right) \otimes \mathbf{F}_{\text{BS},0}^H \chi_{\text{BS},k}^{[m]}, \quad (37)$$

where $\mathbf{F}_{\text{MS},0}^{[m-1]}$ denotes the uplink beamformer designed based on $\hat{\phi}_0^{[m-1]}$ and its uncertainty obtained from the covariance of the corresponding term from the EKF, i.e., the first diagonal element of the covariance estimate of $\psi_{\text{dl},0}^{[m]} = [\phi_0^{[m]}, \dot{\phi}_0^{[m]}]^T$ denoted by $[\mathbf{P}_{\psi_{\text{dl},0}}^{[m-1|m-1]}]_{1,1}$ as will be described in Section V. The terms $\chi_{\text{BS},k}^{[m]}$ and $\chi_{\text{MS},k}^{[m]}$ denote the vectors $\chi_{\text{BS},k}$ and $\chi_{\text{MS},k}$ evaluated at $\theta_k^{[m]}$ and $\phi_k^{[m]}$, respectively. The delay vector is defined as $\mathbf{a}(\tau_k) = [1, \dots, e^{-j2\pi(N-1)\tau_k/(NT_s)}]^T$, and $\mathbf{X}_0 = [\mathbf{x}^{(0)}[0], \dots, \mathbf{x}^{(0)}[N-1]]^T$

¹⁴The acceleration terms $\ddot{\theta}_0^{[m]}$, $\ddot{\phi}_0^{[m]}$, and $\ddot{\tau}_0^{[m]}$ can be incorporated in (33) and defined as $\ddot{\tau}_0^{[m]} = (\dot{\tau}_0^{[m]} - \dot{\tau}_0^{[m-1]})/T_B$, $\ddot{\theta}_0^{[m]} = (\dot{\theta}_0^{[m]} - \dot{\theta}_0^{[m-1]})/T_B$, and $\ddot{\phi}_0^{[m]} = (\dot{\phi}_0^{[m]} - \dot{\phi}_0^{[m-1]})/T_B$, respectively, and initialized similarly.

¹⁵If the rates of change for the AOA and AOD during the tracking phase are equal, then it is sufficient to use only the uplink transmission as the measurement equation. This is due to the fact that the rotation angle can be obtained as a direct consequence of (40).

where $\mathbf{x}^{(0)}[n]$ is the $M_{\text{MS}} \times 1$ vector of simultaneously transmitted symbols for the n -th subcarrier for the LOS link. Similarly, the measurement equation in the downlink is obtained for all the subcarriers for the designed beamformers towards the LOS as

$$\tilde{\mathbf{y}}_r^{\text{dl},[m]} = \boldsymbol{\vartheta}_0^{\text{dl}}(\boldsymbol{\eta}_0^{[m]}) + \sum_{l=1}^{\hat{K}} \boldsymbol{\vartheta}_0^{\text{dl}}(\boldsymbol{\eta}_l^{[m]}) + \tilde{\mathbf{n}}_{\text{MS}}^{[m]}, \quad (38)$$

where $\boldsymbol{\vartheta}_0^{\text{dl}}(\boldsymbol{\eta}_l^{[m]})$ is obtained similar to (37), by replacing the subscripts MS and BS with BS and MS, respectively. The term $\phi_0^{[m]}$ is the parameter to be tracked in the MS, and the downlink beamformer $\mathbf{F}_{\text{BS},0}^{[m-1]}$ is designed based on $\hat{\theta}_0^{[m-1]}$ and its uncertainty obtained from the covariance of the corresponding term from the EKF, i.e., the second diagonal element of the covariance estimate of $\boldsymbol{\psi}_{\text{ul},0}^{[m]} = [\tau_0^{[m]}, \theta_0^{[m]}, \dot{\tau}_0^{[m]}, \dot{\theta}_0^{[m]}]^T$ denoted by $[\mathbf{P}_{\boldsymbol{\psi}_{\text{ul},0}}^{[m-1|m-1]}]_{2,2}$ detailed in Section V. In summary, the tracking phase starts in the uplink by transmission of the beams towards the LOS using the AOA information obtained from the training phase in the downlink, then the TOA/AOA are tracked at the BS. Using the TOA/AOA in the uplink, the BS computes the location of the MS. Finally, using the location information and tracked AOA in the downlink, the MS tracks its rotation angle. The procedure is repeated within the observation time based on the information obtained from the previous tracking block.

B. Conversion to Position and Orientation

Using the channel parameters after tracking in $\{\hat{\tau}_0^{[m]}, \hat{\theta}_0^{[m]}, \hat{\phi}_0^{[m]}\}$, the tracked values of position and rotation angle $\{\hat{\mathbf{p}}^{[m]}, \hat{\alpha}^{[m]}\}$ can be obtained using the following equations for the LOS path

$$\hat{\mathbf{p}}^{[m]} = \mathbf{q} + c\hat{\tau}_0^{[m]} \left[\cos(\hat{\theta}_0^{[m]}), \sin(\hat{\theta}_0^{[m]}) \right]^T, \quad (39)$$

$$\hat{\alpha}^{[m]} = \pi + \hat{\theta}_0^{[m]} - \hat{\phi}_0^{[m]}. \quad (40)$$

The uncertainty of position $\mathbf{P}_{\mathbf{p}}^{[m|m]}$ and rotation angle $P_{\alpha}^{[m|m]}$ are computed as

$$\mathbf{P}_{\mathbf{p}}^{[m|m]} = \left(\mathbf{T}(\hat{\tau}_0^{[m]}, \hat{\theta}_0^{[m]}) \left[\mathbf{P}_{\boldsymbol{\psi}_{\text{ul},0}}^{[m|m]} \right]_{1:2,1:2}^{-1} \mathbf{T}^T(\hat{\tau}_0^{[m]}, \hat{\theta}_0^{[m]}) \right)^{-1}, \quad (41)$$

$$P_{\alpha}^{[m|m]} = \left[\mathbf{P}_{\boldsymbol{\psi}_{\text{ul},0}}^{[m|m]} \right]_{2,2} + \left[\mathbf{P}_{\boldsymbol{\psi}_{\text{dl},0}}^{[m|m]} \right]_{1,1}, \quad (42)$$

where $\mathbf{T}(\hat{\tau}_0^{[m]}, \hat{\theta}_0^{[m]})$ denotes the conversion matrix $\mathbf{T}(\tau_0, \theta_0) = \left[\frac{\partial \tau_0}{\partial \mathbf{p}}, \frac{\partial \theta_0}{\partial \mathbf{p}} \right]$ evaluated at $(\hat{\tau}_0^{[m]}, \hat{\theta}_0^{[m]})$ with

$$\frac{\partial \tau_0}{\partial \mathbf{p}} = \frac{1}{c} [\cos(\theta_0), \sin(\theta_0)]^T, \quad (43)$$

$$\frac{\partial \theta_0}{\partial \mathbf{p}} = \frac{1}{c\tau_0} [-\sin(\theta_0), \cos(\theta_0)]^T. \quad (44)$$

The operation $[\cdot]_{1:2,1:2}^{-1}$ in (41) denotes the 2×2 upper left submatrix of the inverse of the argument. In principle, the information from the LOS link (i.e., equations (39)-(40)) is sufficient to track user

position and rotation angle $\{\hat{\mathbf{p}}^{[m]}, \hat{\alpha}^{[m]}\}$ with an acceptable accuracy. Moreover, gaining the NLOS links information to improve position and rotation angle accuracies in the tracking phase requires *simultaneous* transmission of the beams in the LOS and NLOS directions. A method for tracking of the channel parameters with simultaneous transmission of the beams in the LOS and NLOS was introduced in [39]. This method led to the reduced channel parameter accuracy compared to the link by link tracking [38]. In addition, for the special cases that tracking information from the NLOS links helps to improve the localization accuracy, it also considerably increases the number of required RF chains. This is due to the fact that more than one beams are required to be transmitted in the direction of each first-order reflector to ensure a certain angular support during the tracking. Thus, a simplified position and rotation angle tracking system uses the information provided by the LOS link *only* with the tracking time¹⁶ $T_{\text{track}} = 2T_s$. Moreover, the position and rotation angle tracking accuracies are significantly reduced when the LOS link is blocked [43], [55]. So, the LOS link is used for tracking position and rotation angle and either LOS detection methods or online blockage identification approaches can be adopted depending on the applications¹⁷ [57]–[61]. This allows to simply switch to the BS that is in the LOS thanks to the ultra dense networks.

V. HEURISTIC BEAMFORMER FOR TRACKING

Previously, the robust beamformer design based on the minimization of the Cramér-Rao bound (CRB) of the AOA/AOD for maximum angular spreads $\sigma_{\theta_0}^{\max}$ and $\sigma_{\phi_0}^{\max}$ was proposed in [62]. We propose a much simpler approach named as heuristic beamformers in beamspace. The proposed method does not require any optimization and relies on the angular support during the tracking phase. It is assumed that the beamformer \mathbf{F}_{MS} in the downlink is designed based on the maximum angular spread $\sigma_{\phi_0}^{\max}$. A similar process can be performed for the beamformer \mathbf{F}_{BS} in the uplink based on the maximum angular spread $\sigma_{\theta_0}^{\max}$. Moreover, the design of beamformers $\mathbf{F}_{\text{MS}}^{[m-1]}$ in the uplink based on $\hat{\phi}_0^{[m-1]}$ and its uncertainty $[\mathbf{P}_{\psi_{\text{dl},0}}^{[m-1|m-1]}]_{1,1}$, and $\mathbf{F}_{\text{BS}}^{[m-1]}$ in the downlink based on $\hat{\theta}_0^{[m-1]}$ and the uncertainty $[\mathbf{P}_{\psi_{\text{ul},0}}^{[m-1|m-1]}]_{2,2}$ follows a similar procedure. Finally, joint heuristic beamforming and channel estimation-tracking algorithm is proposed at the end of this section.

¹⁶Note that due to the simultaneous transmission of beams $M_{\text{ms}} \ll G$ in the uplink the tracking time is significantly reduced compared to the training time, i.e., $GT_{\text{track}} \approx T_{\text{train}}$.

¹⁷As an example, blockage can be modeled based on 2-D knife edge diffraction [56]. This allows the receiver to apply a transient change detection algorithm based on the mean change of a complex Gaussian distribution as the signal integrity metric for the LOS blockage identification [57].

A. Beamformer Design Problem

We consider any time slots $[0, T_{\text{ob}})$ where T_{ob} denotes the maximum duration for tracking phase, i.e., the observation time interval. The robust beamformer design within observation time interval $[0, T_{\text{ob}})$ can be formulated as

$$\mathcal{R}_B : \underset{\mathbf{F}_{\text{MS}}}{\text{minimize}} \quad \underset{(\theta_0, \phi_0) \in \mathcal{R}_{\theta_0} \times \mathcal{R}_{\phi_0}}{\text{maximize}} \quad \text{maximize} \left\{ \mathbb{E} \left[(\hat{\theta}_0 - \theta_0)^2 \right], \mathbb{E} \left[(\hat{\phi}_0 - \phi_0)^2 \right] \right\} \quad (45a)$$

$$\text{subject to} \quad \mathbb{E} [\hat{\boldsymbol{\eta}}_0] = \boldsymbol{\eta}_0, \quad (45b)$$

where \mathcal{R}_{θ_0} and \mathcal{R}_{ϕ_0} denote the ranges of θ_0 and ϕ_0 for the maximum angular spreads $\sigma_{\theta_0}^{\text{max}}$ and $\sigma_{\phi_0}^{\text{max}}$, respectively, and the constraint (45b) guarantees the estimation of the channel parameters for the LOS path $\hat{\boldsymbol{\eta}}_0$ to be unbiased. The expectations and unbiased constraints in \mathcal{R}_B can be replaced using the equivalent terms from the FIM. Consequently, the robust beamformer $\mathbf{F}_{\text{MS}} = \mathbf{F}_{\text{RF,MS}} \mathbf{F}_{\text{BB,MS}}$ is designed for maximum angular spreads $\sigma_{\theta_0}^{\text{max}}$ and $\sigma_{\phi_0}^{\text{max}}$ within the observation time T_{ob} [62].

B. Heuristic Beamformer

To provide angular support of the robust beamformer within the observation time T_{ob} for the LOS [62], one needs to use the estimated AOA in the downlink from the training phase. Then, the heuristic beamformer for even and odd number of transmitted beams M_{MS} are obtained as¹⁸

$$\mathbf{F}_{\text{MS,heu}} = \begin{cases} \mathbf{A}_{\text{odd}} \left(\hat{\phi}_0, \left\{ \hat{\phi}_0 \pm i \Delta \phi_{3\text{dB}} \right\} \right), & M_{\text{MS}} = \text{odd and } i = 1, \dots, \frac{M_{\text{MS}}-1}{2} \\ \mathbf{A}_{\text{even}} \left(\hat{\phi}_0 \pm 0.5 \Delta \phi_{3\text{dB}}, \left\{ \hat{\phi}_0 \pm i \Delta \phi_{3\text{dB}} \right\} \right), & M_{\text{MS}} = \text{even and } i = 2, \dots, \frac{M_{\text{MS}}}{2} \end{cases} \quad (46)$$

where $\mathbf{A}_{\text{odd}} \left(\hat{\phi}_0, \left\{ \hat{\phi}_0 \pm i \Delta \phi_{3\text{dB}} \right\} \right)$ and $\mathbf{A}_{\text{even}} \left(\hat{\phi}_0 \pm 0.5 \Delta \phi_{3\text{dB}}, \left\{ \hat{\phi}_0 \pm i \Delta \phi_{3\text{dB}} \right\} \right)$ denote the $N_{\text{MS}} \times M_{\text{MS}}$ matrices with 3 dB beam overlap, the columns formed as shifted versions of $\mathbf{a}_{\text{MS}}(\hat{\phi}_0)$, and even and odd number of beams, respectively, the value of M_{MS} should approximately satisfy $M_{\text{MS}} \geq \lceil \sigma_{\phi_0}^{\text{max}} N_{\text{MS}} / 2 \rceil$ for the symmetric coverage of the maximum angular spread of $\sigma_{\phi_0}^{\text{max}}$ centered around $\hat{\phi}_0$, and $\Delta \phi_{3\text{dB}}$ denotes the phase shift to provide the 3 dB beam overlap for the uniform linear array (ULA) [63]. As an example, for the maximum angular spread of $\sigma_{\phi_0}^{\text{max}} [\text{deg}] = 20$ centered around $\hat{\phi}_0$ and $N_{\text{MS}} = 32$, one needs at least $M_{\text{MS}} = 6$ beams. In principle, heuristic beamformer is obtained by forming M_{MS} beams centered around the estimated AOA in the downlink obtained from the training phase. Since, the 3 dB beam overlap is applied the best spatial coverage is obtained in the tracking phase.

¹⁸The transmit beamformers in the downlink and uplink are obtained similarly using the sequential transmission in case of limited number of RF chains, or transmission in parallel otherwise.

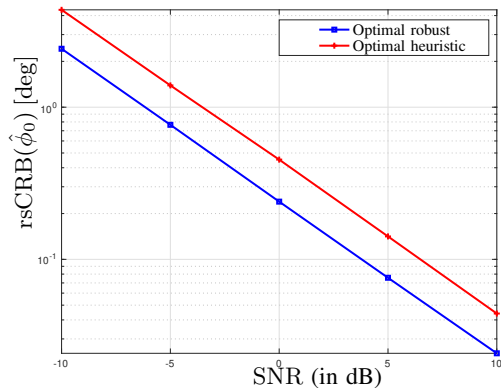


Fig. 3: Comparison between the performance of robust and heuristic beamformers versus SNR.

C. Numerical Comparison

Unlike the method in [62] for the robust beamformer design, the proposed heuristic solution does not require to solve a complex optimization problem. The performance in terms of root-square CRB (rsCRB) for the maximum angular spread of $\sigma_{\phi_0}^{\max}$ [deg] = 20 is compared in Fig. 3. It is observed that the heuristic design leads to around 50% relative increase of $\text{rsCRB}(\hat{\phi}_0)$ [deg] as the price for reducing the complexity compared to the robust counterparts.

D. Hybrid Design

Similar to [64], the hybrid design solution for the proposed heuristic beamformer in (46) is obtained using sparsity constrained matrix reconstruction problem that can be solved using the orthogonal matching pursuit (OMP) type algorithms. Consequently, the baseband precoder is obtained by M_{MS} nonzero rows of $\mathbf{F}_{\text{BB,MS}}$ with M_{MS} columns and $\mathbf{F}_{\text{RF,MS}}$ is given by the corresponding columns of \mathbf{U}_{MS} for the ideal beam selection, and mapped to the closest 1-bit beamformer with $\{+1, -1\}$ for 1-bit beam selection [65].

E. Heuristic Beamforming and Position and Orientation Training-Tracking

The heuristic beamforming and position and orientation training-tracking algorithm is summarized in the Algorithm 2. In step 2, the estimated channel parameters $\hat{\boldsymbol{\eta}}_0^{[m-1]} = [\hat{\tau}_0^{[m-1]}, \hat{\theta}_0^{[m-1]}, \hat{\phi}_0^{[m-1]}]^T$ and corresponding values of the position $\hat{\mathbf{p}}^{[m-1]}$ and rotation angle $\hat{\alpha}^{[m-1]}$ are obtained¹⁹. In step 3, the heuristic hybrid beamformer with 1-bit phase shifters is applied for the tracking phase for the receiver in

¹⁹For $m = 1$, these values are obtained from the training phase, and for $m > 1$ they are obtained from the tracking phase.

Algorithm 2: Heuristic Beamforming and Position and Orientation Training-Tracking

Input : Set $m = 1$, and T_{ob} .

Output: Tracked position $\hat{\mathbf{p}}^{[m]}$ and rotation angle $\hat{\alpha}^{[m]}$ within T_{ob} with the corresponding uncertainties in (41) and (42), respectively.

1 **repeat**

2 Compute $\hat{\tau}_0^{[m-1]}$ and $\hat{\theta}_0^{[m-1]}$ in the BS, $\hat{\phi}_0^{[m-1]}$ in the MS, and the corresponding values of $\hat{\mathbf{p}}^{[m-1]}$ and $\hat{\alpha}^{[m-1]}$ in the training;

3 Hybrid implementation of the received beamformer in the downlink (46) and similarly received beamformer in the uplink;

4 **while** $mT_B \leq T_{\text{ob}}$ **do**

5 Design $\mathbf{F}_{\text{MS}}^{[m-1]}$ in the uplink based on $\hat{\phi}_0^{[m-1]}$ and $[\mathbf{P}_{\psi_{\text{dl},0}}^{[m-1|m-1]}]_{1,1}$;

6 Compute $\hat{\tau}_0^{[m]}$, $\hat{\theta}_0^{[m]}$, and $\hat{\mathbf{p}}^{[m]}$ in the BS;

7 Design $\mathbf{F}_{\text{BS}}^{[m-1]}$ in the downlink based on $\hat{\theta}_0^{[m-1]}$ and $[\mathbf{P}_{\psi_{\text{ul},0}}^{[m-1|m-1]}]_{2,2}$;

8 Compute $\hat{\phi}_0^{[m]}$ in the MS;

9 Using $\hat{\mathbf{p}}^{[m]}$ and $\hat{\phi}_0^{[m]}$, compute $\hat{\alpha}^{[m]}$ in the MS;

10 Set $m = m + 1$;

11 **end**

12 **until** the next observation time T_{ob} ;

the uplink/downlink. In step 5, the uplink beamformer $\mathbf{F}_{\text{MS}}^{[m-1]}$ is designed based on the previous downlink AOA and the corresponding uncertainty. In step 6, the BS tracks the TOA-AOA and the location of the MS in the uplink. In step 7, the downlink beamformer $\mathbf{F}_{\text{BS}}^{[m-1]}$ is designed based on the previous uplink AOA and the corresponding uncertainty. In step 8, the MS tracks the AOA in the downlink. In step 9, the rotation angle is obtained using the location information that is fed back to the MS and the AOA in the downlink, and the block index is updated in step 10 until $mT_B \leq T_{\text{ob}}$. Finally, the steps 2-11 are repeated for the next observation time T_{ob} .

VI. SIMULATION RESULTS

In this section, the performance of the proposed algorithms for different parameters is investigated.

A. Simulation Setup

We consider a scenario representative of indoor localization based on METIS Madrid grid model [66]. We employ the ray tracing simulation tool in order to model the propagation of signals in the

uplink and downlink for channel training and tracking [67]. We set f_c [GHz] = 60, B [MHz] = 200, c [m/ns] = 0.299792, and $N = 40$. The number of transmit and receive antennas are set to $N_{\text{BS}} = 32$ and $N_{\text{MS}} = 32$, respectively, unless otherwise stated. The number of simultaneous beams for the training are set to $M_{\text{BS}} = 1$ and $M_{\text{MS}} = 1$ for the downlink and the uplink, respectively. The number of sequentially transmitted signals for training in the downlink and the uplink satisfies $G \succeq (\hat{K} + 1) \log(N_{\text{MS/BS}} / (\hat{K} + 1))$. Unless otherwise stated, the required number of elements for the SD-based training is set to $V = 3$. Finally, the received SNR in the downlink is defined as

$$\text{SNR} = \frac{\mathbb{E} \left[\left\| \text{blkdiag} \left(\{\boldsymbol{\Omega}_{\text{MS}}[n]\}_{n=0}^{N-1} \right) \text{vec} \left(\{\check{\mathbf{h}}_{\text{MS}}[n]\}_{n=0}^{N-1} \right) \right\|_2^2 \right]}{\mathbb{E} \left[\left\| \text{vec} \left(\{\check{\mathbf{n}}_{\text{MS}}[n]\}_{n=0}^{N-1} \right) \right\|_2^2 \right]}, \quad (47)$$

where $\text{blkdiag}(\cdot)$ creates a block diagonal matrix from its arguments and $\text{vec}(\cdot)$ creates a tall column vector from its arguments. Similarly, the received SNR in the uplink is defined by replacing the subscript MS by BS. During the tracking phase and unless stated otherwise, the MS moves with the velocity on the order of 4 m/s that is in the high range of velocity for indoor localization. Constant angular rates for the UL-AOA and DL-AOA are on the order of $0.4529 \text{ deg}/T_B$ and $0.2265 \text{ deg}/T_B$, respectively. The block duration and the observation time are on the order of T_B [ms] = 10 and T_{ob} [s] = 0.6, respectively. The maximum angular spreads are set to $\sigma_{\theta_0}^{\text{max}}$ [deg] = $\sigma_{\phi_0}^{\text{max}}$ [deg] = 20 centered around $\hat{\theta}_0$ and $\hat{\phi}_0$ within the simulations. During the tracking, M_{MS} in the downlink and M_{BS} in the uplink are set to guarantee the aforementioned maximum angular supports, e.g., $M_{\text{MS}} = 7$ in the downlink and $M_{\text{BS}} = 7$ in the uplink for $N_{\text{BS}} = N_{\text{MS}} = 32$. Unless otherwise stated, the power of the process noise for the continuous-time state model is set to $\mathbf{Q}_c = \text{diag}\{\sigma_{\tau_0}^2, \sigma_{\theta_0}^2, \sigma_{\phi_0}^2\}$ with the standard deviations σ_{τ_0} [ns] = 0.5 and σ_{θ_0} [deg] = σ_{ϕ_0} [deg] = 5, and Φ and $\mathbf{Q}_0^{[m]}$ are obtained by numerical discretization [45].

The performance of the maximum root-mean-square error (RMSE) within the observation time T_{ob} for the estimation and tracking algorithms was assessed from 100 Monte Carlo realizations. The false alarm probability was set to $P_{\text{fa}} = 10^{-3}$ to determine the threshold δ in (24).

B. Results and Discussion

Performance Comparison with Respect to the Adopted CS-Based Estimation for Lens Array: Fig. 4 compares the accuracy in terms of the residual error δ_r of the proposed extended SD-based estimation algorithm 1 with the adopted CS-based estimation for lens array with different values of SNR and the number of elements $V = \{3, 5\}$. It is observed that the residual error in CS-based estimation is approximately twice the corresponding values of the proposed SD-based algorithm. This effect is most pronounced in the low SNR regime, i.e., $\text{SNR} < 0$ dB, as the gap between the residual error of the

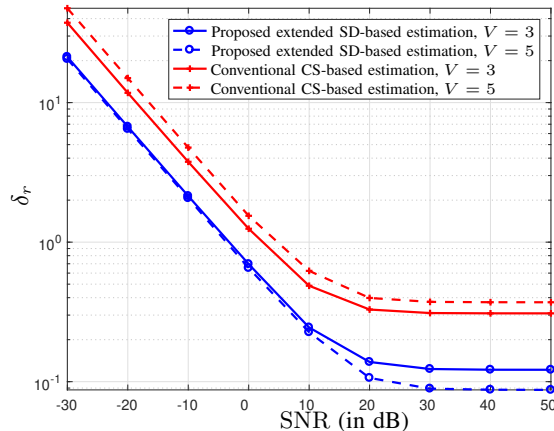


Fig. 4: Residual error for the proposed extended SD-based and conventional CS-based estimations versus SNR for $V = \{3, 5\}$.

proposed extended SD-based algorithm and the CS-based estimation is increased. Moreover, by increasing the number of elements V the error in the CS-based estimation is increased compared to the proposed extended SD-based method. This is due to the reduction of detection probability of the support of the sparse channel coefficient

Performance Comparison with Respect to SNR: Fig. 5 shows the performance of the proposed algorithms for training and tracking for $\text{SNR} [\text{dB}] = \{-10, -5, 0, 5, 10\}$ and $N_{\text{MS}} = N_{\text{BS}} = 32$. The performance of the proposed training and tracking algorithms with heuristic beamformers in the tracking phase with the refinement stated in Section III.C and without refinement in the training phase is compared to the corresponding values of the REB and the PEB within the observation time, i.e., $\forall m \in \mathcal{M}_{\text{ob}}$, for different values of SNR [42], [43]. In Fig. 5 top plot, it is observed that after $\text{SNR} [\text{dB}] = 0$ the maximum value of RMSE of the rotation angle within the observation time saturates to around 5 degrees for the non-refined training and increasing the SNR does not improve the rotation angle estimation accuracy anymore. This is due to the limited number of antenna elements in the BS and the MS. However, using the refinement in the training phase it is possible to approach the corresponding values of the REB without significant saturation. Moreover, the RMSE of the MS position approaches the PEB for $\text{SNR} [\text{dB}] = 0$ within the observation time. The gap between the RMSE of MS position and the PEB within the observation time is mainly due to the limited number of antenna elements in the estimation of AOD as one of the key factors for localization that can be improved by applying the refinement in the training phase as shown in the bottom plot.

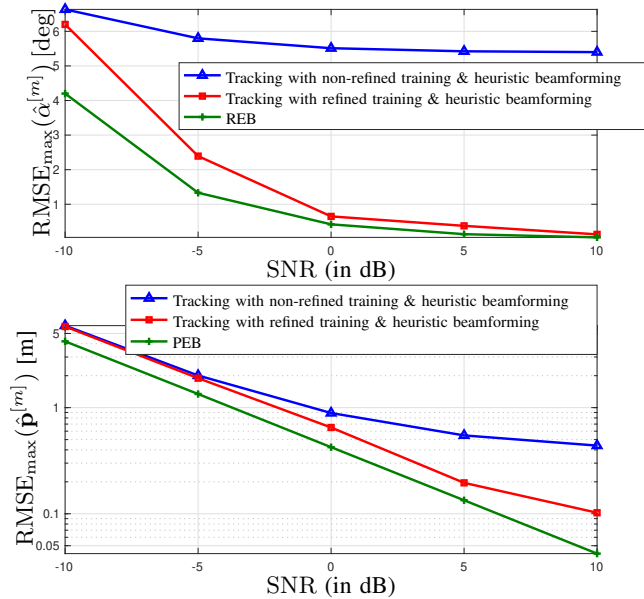


Fig. 5: The maximum RMSE of the MS (top) rotation angle $\hat{\alpha}^{[m]}$, the corresponding REB, (bottom) position $\hat{\mathbf{p}}^{[m]}$, and the corresponding PEB after training with/without refinement and tracking within the observation time $\forall m \in \mathcal{M}_{\text{ob}}$ for SNR [dB] = $\{-10, -5, 0, 5, 10\}$ and $N_{\text{MS}} = N_{\text{BS}} = 32$.

Performance Comparison with Respect to the Number of Antenna Elements: Fig. 6 shows the performance of the training with/without refinement and tracking algorithms for the rotation angle and position of the MS for $N_{\text{MS}} = N_{\text{BS}} = \{20, 32, 64\}$ at SNR [dB] = 0. The performance of the proposed training and tracking algorithms with heuristic beamformer is compared to the corresponding values of the REB and PEB within the observation time for different number of antenna elements [42], [43]. In Fig. 6, the accuracies of the rotation angle and position after training without refinement and tracking in the observation time T_{ob} are mainly limited by the angular resolution that depends on the number of antenna elements, e.g., for $N_{\text{MS}} = N_{\text{BS}} = 32$ it is possible to achieve the rotation angle accuracy of around 5 degrees. This is the main reason for the gap between the proposed method without refinement in the training phase and the corresponding values of the REB and PEB within the observation time. In principle, one can apply the angular refinement procedure in the training phase to obtain closer values to the corresponding REB and PEB as shown with the green bars.

Performance Comparison with Respect to the Power of the Process Noise: Fig. 7 shows the performance of the training with refinement and tracking algorithms using heuristic design with respect to the power of the process noise for the aforementioned rate of changes. It is worth noting that the change of delay only

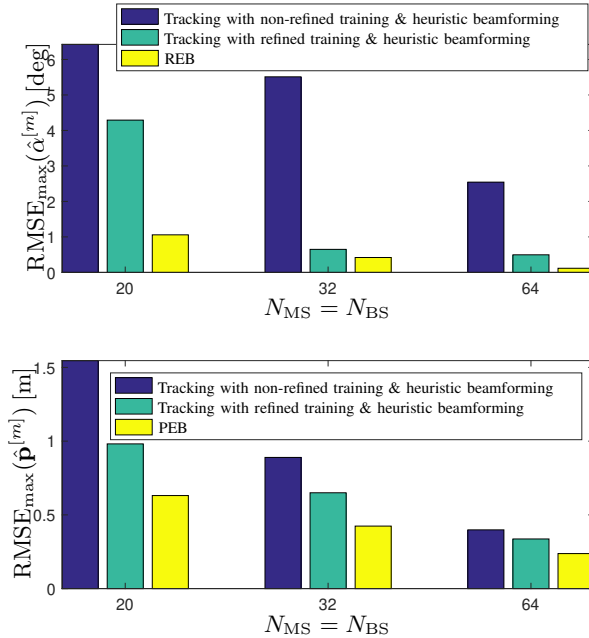


Fig. 6: The maximum RMSE of the MS (top) rotation angle $\hat{\alpha}[m]$ and the corresponding REB, (bottom) position $\hat{\mathbf{p}}^{[m]}$ and the corresponding PEB, after training with/without refinement and tracking within the observation time $\forall m \in \mathcal{M}_{\text{ob}}$ for $N_{\text{MS}} = N_{\text{BS}} = \{20, 32, 64\}$ and SNR [dB] = 0.

affects tracking of the position and does not influence the rotation angle tracking. Consequently, the effects of different values of noise standard deviation of UL-AOA and DL-AOA, i.e., σ_{θ_0} and σ_{ϕ_0} , are analyzed for a given value of σ_{τ_0} . The components of the standard deviation of the process noise for the continuous-time state model \mathbf{Q}_c are set to σ_{τ_0} [ns] = 0.5 and σ_{θ_0} [deg] = σ_{ϕ_0} [deg] = $\{2, 5, 12.5\}$. For $m > 20$, it is observed that the RMSE of position and rotation angle gradually increases versus the block index by increasing the standard deviations of UL-AOA and DL-AOA to σ_{θ_0} [deg] = σ_{ϕ_0} [deg] = 12.5 compared to the estimated values, i.e., block index zero. This is mainly due to the limited angular support of the received beamformers designed based on the maximum angular spreads $\sigma_{\theta_0}^{\text{max}}$ [deg] = $\sigma_{\phi_0}^{\text{max}}$ [deg] = 20. On the other hand, for low to average values of the standard deviations of UL-AOA and DL-AOA on the order of σ_{θ_0} [deg] = σ_{ϕ_0} [deg] = $\{2, 5\}$ the RMSE of position and rotation angle are close to the values obtained from the training during $1 \leq m < 60$, i.e., block index zero. The main reason is that the user is mostly moving within the the angular support of the received beamformers. For $m \geq 60$ and σ_{θ_0} [deg] = σ_{ϕ_0} [deg] = 5, the user starts to move out of the angular support that leads to increasing the RMSE.

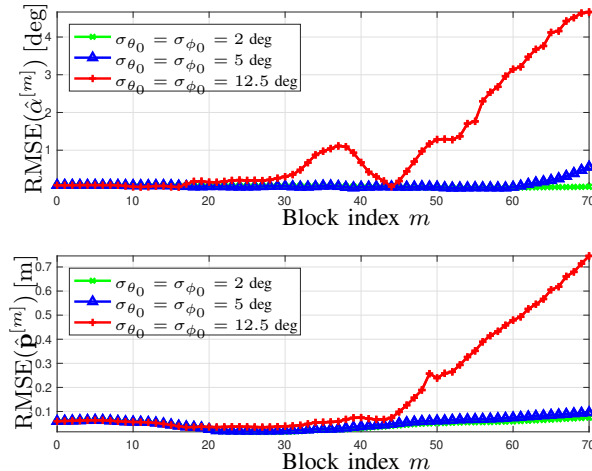


Fig. 7: The RMSE of the MS (top) rotation angle $\hat{\alpha}^{[m]}$ and (bottom) position $\hat{\mathbf{p}}^{[m]}$ with the given rate of changes, and the standard deviation of the process noise with the diagonal components of σ_{τ_0} [ns] = 0.5 and σ_{θ_0} [deg] = σ_{ϕ_0} [deg] = {2, 5, 12.5} after training with refinement for the first 70 block indices with $N_{\text{MS}} = N_{\text{BS}} = 32$ and SNR [dB] = 10.

Performance Comparison with the Method in [38]: For the sake of comparison, the method in [38] is adopted to the more complete state model including the rate of change terms in (34) with lens antenna arrays in the transmitter and receiver for σ_{τ_0} [ns] = 0.5 and σ_{θ_0} [deg] = σ_{ϕ_0} [deg] = {2, 5}. In Fig. 8, it is observed that the proposed method provides a more robust performance for position and rotation angle tracking within the observation time. This is mainly due to the fact that the received beamformers in the proposed method are designed based on the maximum angular spreads in the uplink and downlink. For σ_{θ_0} [deg] = σ_{ϕ_0} [deg] = 2 and $m > 70$, the user is out of the angular support in the proposed method and starts diverging from the trajectory. By increasing the angular spreads to σ_{θ_0} [deg] = σ_{ϕ_0} [deg] = 5, diverging from the trajectory occurs slightly faster at $m > 60$ in the proposed method. In [38], the design is not based on the maximum angular spreads. This leads to beam misalignment and non-robust performance compared to the proposed method and consequently faster divergence from the trajectory.

VII. CONCLUSION

We have studied the determination of a receiver position and orientation using a single transmitter in a mm-wave MIMO system with lens antenna arrays. Our study includes novel solutions for training the mm-wave lens MIMO channel, tracking position and orientation, and heuristic beamformer design. We have proposed a novel method for training of the mm-wave lens MIMO channel with the reduced training

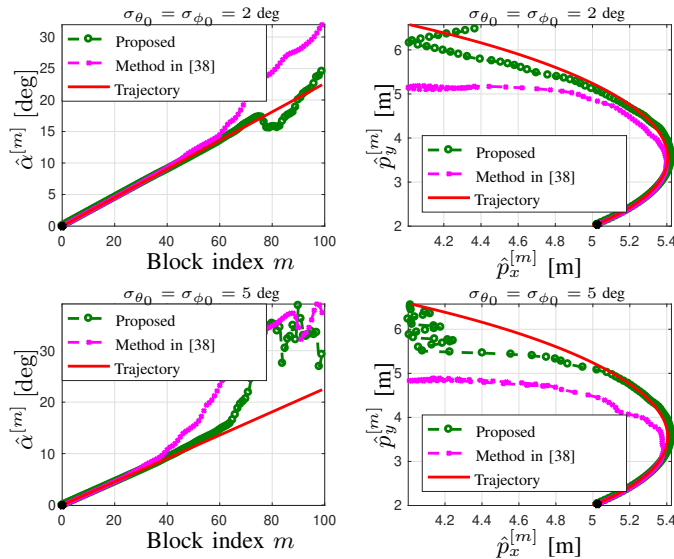


Fig. 8: The trajectory of the MS rotation angle $\hat{\alpha}[m]$, and position $\hat{\mathbf{p}}[m]$ with $N_{\text{MS}} = N_{\text{BS}} = 32$ and $\text{SNR} [\text{dB}] = 10$ compared to the method in [38] for (top) $\sigma_{\theta_0} [\text{deg}] = \sigma_{\phi_0} [\text{deg}] = 2$, and (bottom) $\sigma_{\theta_0} [\text{deg}] = \sigma_{\phi_0} [\text{deg}] = 5$. The black stars show the estimated position and rotation angle from the training.

time. A simplified approach named heuristic beamformer design was proposed for position and orientation tracking. The proposed heuristic beamformer does not require to solve complex optimization problems. Using the proposed heuristic design and tracking algorithm, a joint beamformer design and position and orientation tracking method was proposed. Through simulation studies, we have demonstrated the efficiency of the proposed algorithms, and have shown that the proposed training and joint beamformer design and tracking methods provide practical solutions for updating the location information of the user in dynamic conditions. In particular, the performance of the proposed position and rotation angle tracking is close to the estimated values during the observation time without re-estimating channel parameters for different blocks with much reduced complexity.

VIII. COMPLEXITY ANALYSIS

We analyze the complexity of different stages of the proposed training phase.

- Algorithm 1: The complexity in performing (25) is on the order of $O(N_{\text{MS}}GN_{\text{sub}})$ where N_{sub} denotes the few subcarriers sufficient to detect the dominant path. The LS solution in (28) can be computed with the complexity on the order of $O(GNV^2)$ for all the subcarriers. The complexity of the matrix $\bar{\mathbf{F}}_{\text{MS},x}[n]$ of size $G \times N_{\text{MS}}$ multiplied by the vector $\hat{\mathbf{h}}_{\text{MS},t}[n] \big|_{\text{supp}(\chi_{\text{MS},t})}$ of size $N_{\text{MS}} \times 1$

in (29) is on the order of $O(GNN_{\text{MS}})$ for all the subcarriers. Finally, the complexity in computing τ_k is on the order of $O(ND_o\hat{K})$ where D_o denotes the number of delay grid points, and computing \tilde{h}_k requires $O(N\hat{K})$ operations. Consequently, the maximum complexity of the Algorithm 1 is dominated by the term $\hat{K} \times O(GNN_{\text{MS}})$.

- AOA estimation in the uplink: Similarly, the total complexity for the estimation of AOA in the uplink is dominated by the term $\hat{K} \times O(N_{\text{BS}}GN_{\text{sub}})$.

Following the above discussion²⁰, the overall complexity for channel training is approximately on the order of $\hat{K} \times (O(GNN_{\text{MS}}) + O(N_{\text{BS}}GN_{\text{sub}}))$.

REFERENCES

- [1] P. Zhouyue and F. Khan, "An introduction to millimeter-wave mobile broadband systems," *IEEE Commun. Mag.*, vol. 49, no. 6, pp. 101–107, Jun 2011.
- [2] T. Rappaport, S. Sun, R. Mayzus, H. Zhao, Y. Azar, K. Wang, G. Wong, J. Schulz, M. Samimi, and F. Gutierrez, "Millimeter wave mobile communications for 5G cellular: It will work!" *IEEE Access*, vol. 1, pp. 335–349, May 2013.
- [3] J. Wang, "Beam codebook based beamforming protocol for multi-Gbps millimeter-wave WPAN systems," *IEEE J. Sel. Areas Commun.*, vol. 27, no. 8, pp. 1390–1399, Oct 2009.
- [4] S. Hur, T. Kim, D. Love, J. Krogmeier, T. Thomas, and A. Ghosh, "Millimeter wave beamforming for wireless backhaul and access in small cell networks," *IEEE Trans. Commun.*, vol. 61, no. 10, pp. 4391–4403, Oct 2013.
- [5] Y. Tsang, A. Poon, and S. Addepalli, "Coding the beams: Improving beamforming training in mmwave communication system," in *Global Commun. Conf. (GLOBECOM)*, Kathmandu, Nepal, Dec 2011, pp. 1–6.
- [6] J. Brady, N. Behdad, and A. Sayeed, "Beamspace MIMO for millimeter-wave communications: System architecture, modeling, analysis, and measurements," *IEEE Trans. Antennas Propag.*, vol. 61, no. 7, pp. 3814–3827, Jul 2013.
- [7] J. H. Brady and A. Sayeed, "Wideband communication with high-dimensional arrays: New results and transceiver architectures," in *IEEE International Conference on Communication (ICC)*, London, UK, Jun 2015, pp. 1042–1047.
- [8] M. T. Martinez-Ingles, D. P. Gaillot, J. Pascual-Garcia, J. M. Molina-Garcia-Pardo, M. Lienard, and J. V. Rodriguez, "Deterministic and experimental indoor mmW channel modeling," *IEEE Antennas Wireless Propag. Lett.*, vol. 13, pp. 1047–1050, May 2014.
- [9] R. G. Vaughan and J. B. Andersen, *Channels, Propagation and Antennas for Mobile Communications*. London, UK: Institute of Electrical Engineers (IEE), 2003.
- [10] mmMAGIC White Paper 2.1, "Measurement campaigns and initial channel models for preferred suitable frequency ranges," <https://5g-mmmagic.eu/>, vol. version 1.0, Mar 2016.
- [11] Z. Marzi, D. Ramasamy, and U. Madhow, "Compressive channel estimation and tracking for large arrays in mm-wave picocells," *IEEE J. Sel. Topics. Signal Process.*, vol. 10, no. 3, pp. 514–527, Apr 2016.
- [12] J. Lee, G.-T. Gil, and Y. H. Lee, "Channel estimation via orthogonal matching pursuit for hybrid MIMO systems in millimeter wave communications," *IEEE Trans. Commun.*, vol. 64, no. 6, pp. 2370–2386, Jun 2016.

²⁰To reduce the computational complexity in the MS, it is possible to start the training phase in the uplink for joint estimation of the AOA and TOA at the BS. Due to channel reciprocity, the same algorithms in the training phase can be easily adopted in this case.

- [13] A. Alkhateeb, O. E. Ayach, G. Leus, and R. W. Heath Jr., “Channel estimation and hybrid precoding for millimeter wave cellular systems,” *IEEE J. Sel. Topics. Signal Process.*, vol. 8, no. 5, pp. 831–846, Oct 2014.
- [14] J. Choi, “Beam selection in mm-wave multiuser MIMO systems using compressive sensing,” *IEEE Trans. Commun.*, vol. 63, no. 8, pp. 2936–2947, Aug 2015.
- [15] A. Alkhateeb, O. E. Ayach, G. Leus, and R. W. Heath Jr., “Compressed-sensing based multi-user millimeter wave systems: How many measurements are needed?” in *Proc. IEEE Int. Conf. Acoustics, Speech and Sig. Process. (ICASSP)*, Brisbane, QLD, Australia, Apr 2015, pp. 2909–2913.
- [16] Y. Han and J. Lee, “Two-stage compressed sensing for millimeter wave channel estimation,” in *Proc. IEEE Int. Symp. on Inform. Theory (ISIT)*, Barcelona, Spain, Jul 2016, pp. 860–864.
- [17] J. Lee, G.-T. Gil, and Y. Lee, “Exploiting spatial sparsity for estimating channels of hybrid MIMO systems in millimeter wave communications,” in *Proc. IEEE Global Commun. Conf. (GLOBECOM)*, Austin, TX, USA, Dec 2014, pp. 3326–3331.
- [18] D. Ramasamy, S. Venkateswaran, and U. Madhow, “Compressive adaptation of large steerable arrays,” in *Proc. IEEE Inform. Theory and Applicat. Workshop (ITA)*, San Diego, CA, USA, Feb 2012, pp. 234–239.
- [19] D. E. Berraki, S. M. D. Armour, and A. R. Nix, “Application of compressive sensing in sparse spatial channel recovery for beamforming in mmwave outdoor systems,” in *Proc. IEEE Wireless Commun. and Networking Conf. (WCNC)*, Istanbul, Turkey, Apr 2014, pp. 887–892.
- [20] M. F. Duarte, S. Sarvotham, D. Baron, M. B. Wakin, and R. G. Baraniuk, “Distributed compressed sensing of jointly sparse signals,” in *Proc. 39th Asilomar Conf. Sig., Syst., Comp.*, Pacific Grove, CA, USA, Oct 2005, pp. 1537–1541.
- [21] M. F. Duarte, V. Cevher, and R. G. Baraniuk, “Model-based compressive sensing for signal ensembles,” in *Proc. 47th Ann. Allerton Conf. Communication, Control, Computing, (Monticello, IL)*, Monticello, IL, USA, Sep 2009, pp. 244–250.
- [22] Y. C. Eldar, P. Kuppinger, and Bolcskei, “Block-sparse signals: Uncertainty relations and efficient recovery,” *IEEE Trans. Signal Processing*, vol. 58, no. 6, pp. 3042–3054, Jun 2010.
- [23] X. Gao, L. Dai, S. Han, C.-L. I, and R. Heath Jr., “Energy-efficient hybrid analog and digital precoding for mmWave MIMO systems with large antenna arrays,” *IEEE J. Sel. Areas Commun.*, vol. 34, no. 4, pp. 998–1009, Apr 2016.
- [24] Y. Zeng, R. Zhang, and Z. N. Chen, “Electromagnetic lens-focusing antenna enabled massive MIMO: Performance improvement and cost reduction,” *IEEE J. Sel. Areas Commun.*, vol. 32, no. 6, pp. 1194–1206, Jun 2014.
- [25] Y. Zeng and R. Zhang, “Millimeter wave MIMO with lens antenna array: A new path division multiplexing paradigm,” *IEEE Trans. Commun.*, vol. 64, no. 4, pp. 1557–1571, Apr 2016.
- [26] N. Behdad and A. Sayeed, “Continuous aperture phased MIMO: Basic theory and applications,” in *Proc. Allerton Conference*, Sep 2010, pp. 1196–1203.
- [27] J. Brady, N. Behdad, and A. Sayeed, “Beamspace MIMO for millimeter-wave communications: System architecture, modeling, analysis, and measurements,” *Trans. Antennas Propag.*, vol. 61, no. 7, pp. 3814–3827, Jul 2013.
- [28] X. Gao, L. Dai, S. Han, C. Lin I, and X. Wang, “Reliable beamspace channel estimation for millimeter-wave massive MIMO systems with lens antenna array,” *IEEE Trans. Wireless Commun.*, vol. 16, no. 9, pp. 6010–6021, Sep 2017.
- [29] L. Yang, Y. Zeng, and R. Zhang, “Channel estimation for millimeter wave MIMO communications with lens antenna arrays,” *IEEE Trans. Veh. Technol.* DOI 10.1109/TVT.2017.2779828, Dec 2017.
- [30] J. Hogan and A. Sayeed, “Beam selection for performance-complexity optimization in high-dimension MIMO systems,” in *Conference on Information Sciences and Systems (CISS)*, Princeton, Mar 2016, pp. 337–342.
- [31] J. Wang, J. Liu, T. Pare Jr., T. Wu, G. Bajko, and Y. Hsu, “Direction finding positioning in wireless local area networks,” Mar 2017, US Patent 20170070893. [Online]. Available: <http://www.freepatentsonline.com/y2017/0070893.html>
- [32] P. Sanchis, J. Martinez, J. Herrera, V. Polo, J. Corral, and J. Marti, “A novel simultaneous tracking and direction of arrival

- estimation algorithm for beam-switched base station antennas in millimeter-wave wireless broadband access networks,” in *IEEE Antennas and Propagation Society International Symposium*, San Antonio, TX, USA, USA, Jun 2002, pp. 594–597.
- [33] H. Deng and A. Sayeed, “Mm-wave MIMO channel modeling and user localization using sparse beamspace signatures,” in *International Workshop on Signal Processing Advances in Wireless Communications (SPAWC)*, Toronto, ON, Canada, Jun 2014, pp. 130–134.
- [34] M. Vari and D. Cassioli, “mmWaves RSSI indoor network localization,” in *International Conference on Communication (ICC) Workshop on Advances in Network Localization and Navigation*, Sydney, NSW, Australia, Jun 2014, pp. 127–132.
- [35] A. Hu, T. Lv, H. Gao, Z. Zhang, and S. Yang, “An ESPRIT-based approach for 2-D localization of incoherently distributed sources in massive MIMO systems,” *IEEE J. Sel. Topics Signal Process.*, vol. 8, no. 5, pp. 996–1011, Oct 2014.
- [36] A. Guerra, F. Guidi, and D. Dardari, “Position and orientation error bound for wideband massive antenna arrays,” in *International Conference on Communication (ICC) Workshop on Advances in Network Localization and Navigation*, London, UK, Jun 2015, pp. 853–858.
- [37] V. Savic and E. G. Larsson, “Fingerprinting-based positioning in distributed massive MIMO systems,” in *IEEE Vehicular Technology Conference (VTC)*, Boston, MA, USA, Sep 2015, pp. 1–5.
- [38] V. Va, H. Vikalo, A. Dzul, and R. W. Heath Jr, “Beam tracking for mobile millimeter wave communication systems,” in *IEEE Global Conference on Signal and Information Processing (GlobalSIP)*, Washington, DC, USA, Dec 2016, pp. 743–747.
- [39] C. Zhang, D. Guo, and P. Fan, “Tracking angles of departure and arrival in a mobile millimeter wave channel,” in *IEEE International Conference on Communications (ICC)*, Kuala Lumpur, Malaysia, May 2016, pp. 1–6.
- [40] N. Garcia, H. Wymeersch, E. G. Ström, and D. Slock, “Location-aided mm-wave channel estimation for vehicular communication,” in *Proc. IEEE International Workshop on Signal Processing Advances in Wireless Communications (SPAWC)*, Edinburgh, England, Jul 2016, pp. 1–5.
- [41] N. Garcia, H. Wymeersch, E. G. Larsson, A. M. Haimovich, and M. Coulon, “Direct localization for massive MIMO,” *IEEE Trans. Signal Process.*, vol. 65, no. 10, pp. 2475–2487, May 2017.
- [42] A. Shahmansoori, G. Garcia, G. Destino, G. Seco-Granados, and H. Wymeersch, “5G position and orientation estimation through millimeter wave MIMO,” in *IEEE Global Commun. Conf. (GLOBECOM) Workshop*, San Diego, CA, USA, Dec 2015, pp. 1–6.
- [43] —, “Position and orientation estimation through millimeter wave MIMO in 5G systems,” *IEEE Trans. Wireless Commun.*, vol. 17, no. 3, pp. 1822–1835, Mar 2018.
- [44] J. Li, J. Conan, and S. Pierre, “Position location of mobile terminal in wireless MIMO communication systems,” *J. Commun. Netw.*, vol. 9, no. 3, pp. 254–264, Sep 2007.
- [45] M. Koivisto, M. Costa, J. Werner, K. Heiska, J. Talvitie, K. Leppänen, V. Koivunen, and M. Valkama, “Joint device positioning and clock synchronization in 5G ultra-dense networks,” *IEEE Trans. Wireless Commun.*, vol. 16, no. 5, pp. 2866–2881, May 2017. [Online]. Available: <https://doi.org/10.1109/TWC.2017.2669963>
- [46] M. Koivisto, A. Hakkarainen, M. Costa, P. Kela, K. Leppänen, and M. Valkama, “High-efficiency device positioning and location-aware communications in dense 5G networks,” *IEEE Commun. Mag.*, vol. 55, no. 8, pp. 188–195, 2017. [Online]. Available: <http://ieeexplore.ieee.org/document/7984759/>
- [47] A. Alkhateeb and R. W. Heath, “Frequency selective hybrid precoding for limited feedback millimeter wave systems,” *IEEE Trans. Commun.*, vol. 64, no. 5, pp. 1801–1818, May 2016.
- [48] Y. Zeng and R. Zhang, “Millimeter wave MIMO with lens antenna array: A new path division multiplexing paradigm,” *IEEE Trans. Commun.*, vol. 64, no. 4, Apr. 2016.

- [49] G. Destino and H. Wymeersch, "On the trade-off between positioning and data rate for mm-wave communication," in *IEEE International Conference on Communications Workshops (ICC)*, Paris, France, May 2017, pp. 797–802.
- [50] W. U. Bajwa, J. Haupt, A. Sayeed, and R. Nowak, "Compressed channel sensing: A new approach to estimating sparse multipath channels," *Proceedings of the IEEE*, vol. 98, no. 6, pp. 1058–1076, Jun 2010.
- [51] X. Gao, L. Dai, S. Zhou, A. M. Sayeed, and L. Hanzo, "Beamspace channel estimation for wideband millimeter-wave MIMO with lens antenna array," in *IEEE International Conference on Communications (ICC)*, Kansas, USA, May 2018.
- [52] Y. Bar-Shalom, X. Li, and T. Kirubarajan, *Estimation With Applications to Tracking and Navigation*. Hoboken, NJ, USA: Wiley, 2001.
- [53] N. Czink, X. Yin, H. Özcelik, M. Herdin, E. Bonek, and B. H. Fleury, "Cluster characteristics in a MIMO indoor propagation environment," *IEEE Trans. Wireless Commun.*, vol. 6, no. 4, pp. 1465–1475, Apr 2007.
- [54] X. Yin, T. Pedersen, N. Czink, and B. H. Fleury, "Parametric characterization and estimation of bi-azimuth dispersion path components," in *Proc. of IEEE International Conf. on Signal Processing Advances in Wireless Communications (SPAWC)*, Cannes, France, Jul 2006, pp. 1–6.
- [55] Z. Abu-Shaban, X. Zhou, T. D. Abhayapala, G. Seco-Granados, and H. Wymeersch, "Error bounds for uplink and downlink 3D localization in 5G mmwave systems," *IEEE Trans. Wireless Commun.*, vol. 17, no. 8, pp. 4939–4954, 2018. [Online]. Available: <https://doi.org/10.1109/WTC.2018.2832134>
- [56] W. Qi, J. Huang, J. Sun, Y. Tan, C. X. Wang, and X. Ge, "Measurements and modeling of human blockage effects for multiple millimeter wave bands," in *Wireless Communications and Mobile Computing Conference (IWCMC)*, Valencia, Spain, Jun 2017, pp. 1604–1609.
- [57] D. Egea-Roca, J. A. Lopez-Salcedo, G. Seco-Granados, and H. V. Poor, "Performance bounds for finite moving average tests in transient change detection," *IEEE Trans. Signal Processing*. DOI 10.1109/TSP.2017.2788416, Jan 2018.
- [58] J. Schroeder, S. Galler, K. Kyamakya, and K. Jobmann, "NLOS detection algorithms for ultra-wideband localization," in *IEEE International Conference on Positioning, Navigation, and Communication (WPNC)*, Hannover, Germany, Mar 2007, pp. 159–166.
- [59] M. Basseville and I. V. Nikiforov, *Detection of Abrupt Changes: Theory and Application*. Englewood Cliff: Prentice Hall, 1993.
- [60] H. V. Poor and O. Hadjiladis, *Quickest Detection*. Cambridge University Press, 2009.
- [61] E. Page, "Continuous inspection schemes," *Biometrika*, pp. 100–115, 1954.
- [62] N. Garcia, H. Wymeersch, and D. T. M. Slock, "Optimal robust precoders for tracking the aod and aoa of a mm-wave path," *CoRR*, vol. abs/1703.10978, 2017. [Online]. Available: <http://arxiv.org/abs/1703.10978>
- [63] S. J. Orfanidis, *Electromagnetic Waves and Antennas*. Rutgers University, 2008.
- [64] O. E. Ayach, S. Rajagopal, S. Abu-Surra, Z. Pi, and R. W. Heath Jr, "Spatially sparse precoding in millimeter wave MIMO systems," *IEEE Trans. Wireless Commun.*, vol. 13, no. 3, pp. 1499–1513, Mar 2013.
- [65] D. D. Donno, J. Palacios, and J. Widmer, "Millimeter-wave beam training acceleration through low-complexity hybrid transceivers," *IEEE Trans. Wireless Commun.*, vol. 16, no. 6, pp. 3646–3660, Jun 2017.
- [66] K. e. a. Maltsev, "IEEE doc. 802.11-08/1044r0. 60 GHz WLAN Experimental Investigations," Sep 2008.
- [67] N. Amiot, M. Laaraiedh, and B. Uguen, "PyLayers: An open source dynamic simulator for indoor propagation and localization," in *IEEE International Conference on Communications Workshops (ICC)*, Budapest, Hungary, Jun 2013, pp. 84–88.